

SINGLE PHOTON DETECTION AT TELECOM WAVELENGTH

LIM ZHENG JIE
A0102464R

SUPERVISED BY:
PROFESSOR CHRISTIAN KURTSIEFER

*A thesis submitted for the degree of
Master of Science by Research in Physics*

DEPARTMENT OF PHYSICS
NATIONAL UNIVERSITY OF SINGAPORE

Declaration

I hereby declare that the thesis is my original work and it has been written by me in its entirety. I have duly acknowledged all the sources of information which have been used in the thesis.

The thesis has also not been submitted for any degree in any university previously.

Lim Zheng Jie
December 2018

Acknowledgements

This acknowledgment is probably the most difficult I have ever written, not because it is for a postgraduate thesis, but because the completion of this thesis implies bidding farewell to a group of wonderful people whom I have spent almost four years with.

First, I would like to express my heartfelt gratitude to Professor Christian Kurtz who accepted “Because I heard that you are a very nice professor to work with” as a reason to why I want to join the Quantum Optics group, and thereon, opened the doors for me to the world of Quantum Physics. Working with you has benefitted me in more than just gaining scientific knowledge. Thank you for constantly reassuring me in my potential and complimenting me in every little milestone. Your recognition encourages me to strive for the better.

This arduous journey would not have been as smooth and fruitful if not for the meticulous guidance from my postdoc, Hou Shun. Thank you for being my pillar of strength, giving me courage and determination to continue whenever I am faced with an obstacle.

A million thanks to Victor for being ever-supportive and helpful even though he is no longer in our group. Not forgetting the brainy teammate Yicheng who is always very humble, adorable, and resourceful.

Special mention to Chorng Wang and Imran who played major roles in teaching crucial technical skills which I would not have mastered as quickly if not for their patient guidance. This project would not have been completed without their generous assistance.

Cheers to Chi Huan, Jianwei, and Adrian, my awesome lab mates since the beginning; I will miss the little things we do everyday — deciding on a place for lunch, fighting over the black sofa, making fun of each other, and debating over which coffee place to patronise. I am very fortunate to have your company all these years.

Cheers also to my office-mates, past and present: Chang Hoong, Boon Long,

Matthias, Wilson, and Nick, for all the fun we had in the office. Not forgetting Brenda, who likes to feed me expensive snacks (I love it), and taking extra care of me since we are the only two females in the group. Arigato!

I am also blessed with the support from many people in the Quantum Optics group and the NUS-Singtel cybersecurity project: Assoc Prof Alexander Ling, Alessandro, Lijiong, Mathias, Peng Kian, James, Moe Thar.

Finally, a big thanks to everyone else whom I have crossed paths with in the Centre for Quantum Technologies. I will never forget the fantastic time I spent here!

Last but not least, to you who found this thesis; thank you for taking precious time to read it. I hope you will find this work interesting and useful!

Abstract

Over the past decade, there has been a tremendous increase in interest in new single-photon detector technologies. Manufacturers of single-photon detectors continuously come up with new and better devices that go beyond the capabilities of established detectors. In this work, we investigate the performance of various Indium Gallium Arsenide (InGaAs) single-photon avalanche detectors (SPAD) operating in the Geiger mode. The performance characteristics that are examined include: breakdown voltage, pulse height, dark count rate, detection efficiency, and timing jitter. We also investigate the fluorescence light emitted by the detectors, and discuss ways to suppress it. These InGaAs detectors would eventually be used in the fibre-based Quantum Key Distribution (QKD) system at telecommunication wavelengths (1260 — 1625 nm).

Contents

1	Introduction	1
2	Single Photon Detection with Avalanche Photodiode	7
2.1	Working principle	7
2.1.1	Quenching the avalanche	11
2.1.2	Pulse Discrimination and photon counting	14
2.2	Characteristics of APD	16
2.2.1	Breakdown voltage	16
2.2.2	Pulse height	18
2.2.3	Dark count rate	20
2.2.4	Detection Efficiency	20
2.2.5	Timing Jitter	28
2.3	APD for QKD	32
3	Characterisation of APD	33
3.1	Characterisation of commercial modules	35
3.1.1	ID Quantique ID220-FR	35
3.1.2	Laser Components COUNT Q	47
3.2	Characterisation of bare diodes	50
3.2.1	Princeton Lightwave PGA-016u-1550TFT	52
3.2.2	Renesas NR8360JP-BC	58
3.2.3	Renesas NR8800FS-CB	62
4	Breakdown flash	70
4.1	Detection of Breakdown Flash	71
4.2	Elimination of breakdown flash	76
4.3	Breakdown Flash Probability	77
4.4	Spectral Distribution	79
5	Conclusion and outlook	82

1 Introduction

The issue of secure communication has always been the challenge at heart in the world of information and communication technologies. More countries are beginning to invest in technology that could enable perfectly secure communication. Much attention has been shifted to the implementation of Quantum Key Distribution (QKD), often known as quantum cryptography, for it is widely perceived to have been proved secure in various protocols [1, 2, 3] in contrast to conventional encryption methods.

Quantum Key Distribution provides a means of secure communication where privacy is guaranteed by the laws of physics rather than by computational complexity; the “no-cloning theorem” states that it is impossible to create an identical copy of an unknown quantum state [4]. The sender transmits a cryptographic key which is generated by encoding the quantum state of a series of photons, and the receiver measures the photons in one of the several bases selected at random. Only those measurements made in a basis compatible with the preparation state of photon are used for the key. Due to the no-cloning theorem, eavesdroppers introduce errors into the received key when they attempt to measure (and retransmit) in the wrong basis. The reliance of the *key* is dependent on the quantum bit error rate (QBER), which is based on the percentage of errors within the received key, and is an important factor in determining the security and efficiency of the system. Apart from eavesdroppers, the noise of the system also contributes to QBER.

An encoded qubit then gets detected by devices sensitive to low-intensity light (down to single photon level). Detection of low-intensity light was first made possible when the photoelectric tube (PET) was invented by Elster and Geiter over a century ago in 1913, exploiting the photoelectric effect using visible light to strike alkali metals (potassium and sodium) [5]. Over two decades later, RCA laboratories commercialized the photomultiplier tube (PMT), which marks the start of single photon detection [5].

In a PMT, when light enters the photocathode, one or more photoelectrons are emitted into the vacuum through the external photoelectric effect. These photoelectrons are then accelerated by the focusing electrode voltages towards the

electron multiplier (dynode) where electrons are multiplied through the process of secondary emissions and are collected at the anode as an output signal. Due to secondary emissions which leads to a high overall gain (10^5), PMTs possess extremely high sensitivity relative to other photosensitive devices used to detect light in the ultraviolet, visible, and near infrared regions. Though PMTs offer good single photon detection performance, they require a bias voltage in the order of kilovolts and incorporate fragile vacuum photocathodes and a complicated mechanical structure inside the vacuum container. In addition, PMTs are unable to fulfil the needs of many modern experiments such as quantum computing [6] and lidar imaging [7], which require good detection efficiency and timing resolution that the PMT is also lacking in (the quantum efficiency of a PMT at infrared wavelength is about 1%, and it is very noisy). This triggered the exploration for alternatives to PMTs.

The focus in photodetection techniques soon shifted to the exploration of solid state semiconductor detectors which exploits the robust internal photoelectric effect of a p-n junction in the semiconductor material (to be discussed in detail in the next chapter). Semiconductor-based detectors are promising alternatives to PMTs for they are smaller in size, more robust, and cheaper. Besides, semiconductor-based detectors like the avalanche photodiodes (APD), are matured photodetection technologies that provide inherently higher detection efficiency, particularly in the red and near-infrared spectral regions.

Alternatively, other options such as the transition edge sensors (TES) [8] and superconducting nanowire single-photon detectors (SNSPD) [9] are also excellent choices for low-intensity light detection. Currently, SNSPDs offer the best combination of high detection efficiency ($>70\%$) [10], low false detections (<100 Hz), and high timing resolution (~ 50 ps). However, they require bulky cryogenic refrigeration (<4.2 K), and have small absorber areas of sizes in square microns. TES provides high detection efficiency ($>94\%$) [11] customizable to wavelengths from the millimeter regime to gamma rays [12] and negligible background dark count rate (<10 Hz) from intrinsic thermal fluctuations of the device. However, TES must be operated in a cryogenic environment around 100 mK, and have a low time resolution of approximately 100 ns. Furthermore, a single-photon spike on a TES lasts on the order of microseconds. That said, the choice of a suitable

detector would ultimately depend on the nature of the intended application.

Over the years, much research effort have been committed to building more efficient and robust QKD systems; from the first experimental demonstration of QKD over a short distance of 32cm on an optical table [1], till today where the maximum distance has been increased to up to 400km with academic systems [13], and even the feasibility of satellite-based QKD [14]. Nonetheless, QKD over optical fibres remains as the most practical choice for it has the potential for fast deployment due to existing optical fibre infrastructure and mature telecom technologies to transport encoded photons [15].

In this thesis, we are looking at detectors for fibre-based QKD systems, which would require single-photon detectors that are able to efficiently detect photons at telecom wavelengths (1260 — 1625 nm)¹. As later summarised in this thesis, APD in general offer detection efficiency of approximately 20% and timing jitter in the order of 100 ps. Coupled with good features like compactness, robustness, and lower cost, APD is the detector of choice for the majority of the QKD systems [16, 17, 18].

APDs play a crucial role in QKD systems as their performance affect both the key creation rate as well as the error rate [19]. Although the performance of APDs have already been thoroughly investigated [20, 21], it is observed that two similar detectors can behave differently, thus justifying the need to characterise each and every detector. Ultimately, a deployed large scale fibre-based QKD system would require many detectors to function and it is necessary for one to ensure that the choice of detector is practical and cost-effective.

Since the sensitivity of each semiconductor material of each wavelength is different, APDs made of different materials also have varying spectral response. Silicon avalanche photodiodes (Si-APD) are most commonly used for single photon detection at visible light wavelengths with a quantum efficiency of more than 50% [22]. For single photon detection at telecom wavelengths, Indium Gallium Arsenide (InGaAs) and Germanium (Ge) APDs are the more common choices

¹This wavelength range experiences minimal attenuation over fibres.

despite having relatively higher dark count rates as compared to Si-APDs, and they yield a quantum efficiency of up to 20% [21]. Although significantly more expensive than Ge APDs, InGaAs APDs are typically available with comparatively much lower noise currents and slightly higher quantum efficiency, thus we choose to work with InGaAs APDs in this thesis.

It is crucial to look into any vulnerability of the APDs and find ways to mitigate them. Similar to Si-APDs, InGaAs-APDs exhibit fluorescence from recombination of electron-hole pairs generated in the avalanche breakdown process during detection. This fluorescence, termed as breakdown flash (BDF) or backflash, may open side channels for attacks on QKD systems [23]. BDF has been observed in Si-APDs, which spans over a spectral distribution of 700 nm to 1000 nm [24], and has also been investigated in InGaAs-APDs at specific spectral windows between 1530 nm and 1600 nm [25, 26, 27]. In this thesis, we intend to characterize the BDF from two commercial InGaAs single photon counting modules and study the spectral distribution between 1000 nm and 1600 nm, as well as finding solutions to suppress the BDF.

The first part of this thesis focuses on the characterisation of several commercial photodetection modules and bare diodes for single photon detection at telecommunication wavelengths. The second part of the thesis will look at the detection of BDF of APDs which are potential eavesdropping attack to the QKD system, and discuss methods to suppress them.

2 Single Photon Detection with Avalanche Photodiode

In QKD, information is encoded into a string of photonic qubits which are then received by a single-photon detector. The success of a QKD system thus inherently depends on the ability to detect single photons. In principle, this can be achieved through a variety of techniques, such as photomultiplier tube (PMT), avalanche photodiode (APD), transition edge sensor (TES), and superconducting nanowire single-photon detector (SNSPD). Here, we choose to work with APD for its compactness, robustness, and low cost as compared to other choices which are less economically viable and require a complex system for cooling; a detector that needs liquid helium or nitrogen cooling would certainly render complex commercial development. Hence, it is important to keep the choice of detectors practical.

2.1 Working principle

A photodiode is a semiconductor device that converts light into an electric current through the photoelectric effect. When photons of energy greater than the bandgap of the material are illuminated onto the photodiode, they are absorbed and free charge carriers (electron-hole pairs) are created. The flow of these charge carriers then generates a photocurrent proportional to the received optical power. However, this would imply that low intensity light detection is not possible because the equivalent photocurrent of a few photoelectrons would be too low to be measurable.

The APD has a similar working mechanism but operates at high reversed bias state which enables a single photon to induce a significant amount of free charge carriers making it suitable for low intensity light detection. Most commonly available APDs employ a “reach-through” structure as shown in Figure 3. The diode is reverse-biased above the breakdown voltage (Geiger mode), such that it creates a region of high electric field across the multiplication region.

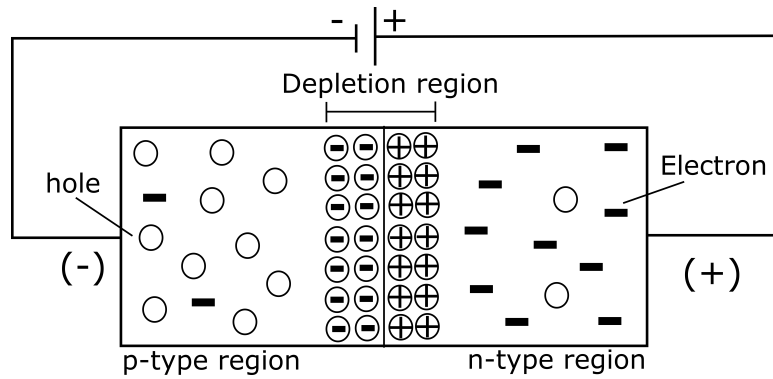


Figure 1: A depletion region of a semiconductor which forms the active region of an APD. The n-type and p-type semiconductor materials are joined together, where n-type is a region of excess free electrons and p-type is a region of excess holes. When both regions are in contact, the electrons and holes recombine at the junction to form a depletion region. The application of a reverse bias to the p-n junction will cause both electrons and holes to be pulled away from the junction.

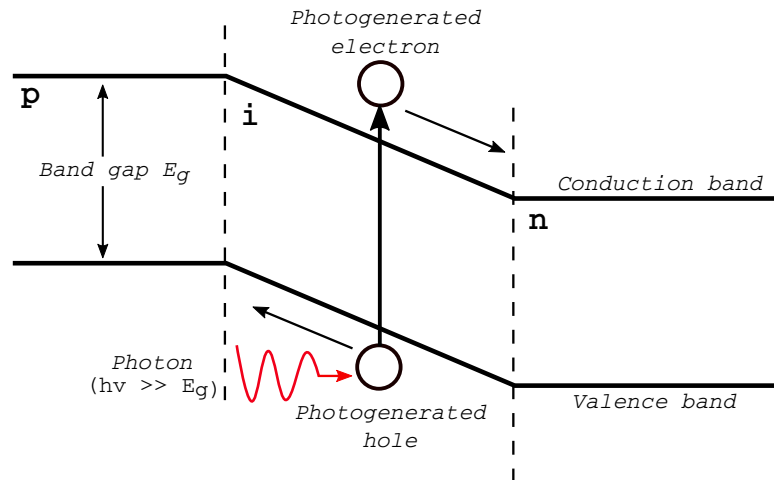


Figure 2: Energy band diagram of a photodiode, illustrating the photoelectric effect. An incident photon of energy more than the bandgap of the semiconductor creates a free electron-hole pair.

When a photon with energy more than the bandgap of the semiconductor strikes the APD, ionization occurs and an electron-hole pair (free charge carriers) is created in the depletion region (photoelectric effect). Under the influence of the electric field, electrons accelerate towards the high electric field region “M” and gain kinetic energy. If the electron gains sufficient energy, collision with atoms in the crystal lattice will create more free electron-hole pairs through impact ionization — the avalanche effect. Eventually, single photoelectrons experience avalanche gains and create millions of photoelectrons which forms macroscopic pulses (photocurrent in the order of nA). The photocurrent translates to a voltage of tens of millivolts across a $50\ \Omega$ load resistor, which makes it easily detectable and relatively easy to discriminate [28].

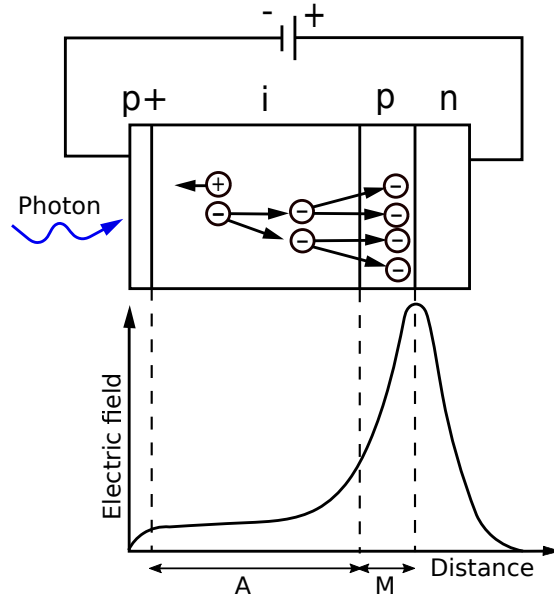


Figure 3: A schematic illustration of the reach-through structure of an avalanche photodiode biased for an avalanche gain. “n” represents a layer of highly doped n-type region; “p” represents a layer of highly doped p-type region; “p+” represents a layer of lightly doped p-type region. “A” represents the absorption region where the free charge carriers are created; “M” represents the multiplication region which is designed to contain a high electric field to achieve a high internal gain. Shown at the bottom is the electric field distribution across the APD regions.

2.1.1 Quenching the avalanche

Initially, the avalanche causes an exponential growth of the current. However, after a period of time, electrons and holes accumulate at the p and n sides of the depletion region respectively, creating an internal electric field in opposition to the applied bias. The current stops growing and remains to flow at I_A (conducting state), disabling the device to detect subsequent photons. In order to detect subsequent photons, the avalanche process must be stopped, and APD has to be brought back into the non-conducting state thereafter. Only then can the APD be operated continuously. The simplest way to accomplish this is through a passive quenching circuit that consists of an high-value ballast resistor R_B connected in series to the diode as shown in Figure 4.

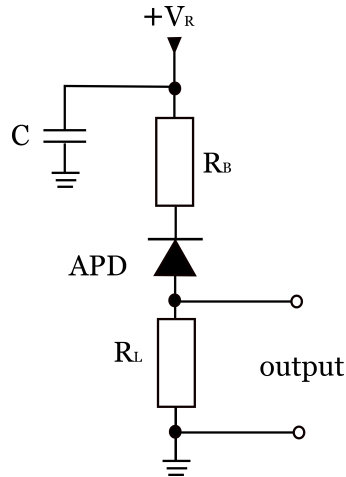


Figure 4: Schematic of a basic passive quenching circuit. The APD is connected in series with a comparatively large ballast resistor R_B , with an applied bias voltage V_R across the series arrangement. The load resistor R_L is for voltage readout.

The external circuit achieves a quenching effect by lowering the avalanche current through discharging the junction capacitance C until the voltage across the APD drops below V_{BDV} . The time taken for the APD to recover to its initial non-conducting state is given by the time constant of the effective RC circuit as represented by equation 1:

$$\tau = R_B C. \quad (1)$$

During this period of time, also known as dead time, the APD is unable to reliably register a second photon.

Some free electrons may have been trapped during the quenching time then released and retrigger the breakdown current as soon as possible. In most cases, τ is deliberately lengthened to suppress this so-called afterpulsing [29] — a spontaneous retriggering of the detector after an initial detection event. Afterpulsing is due to charges, trapped in the deep levels of the semiconductors band structure, released via field-assisted thermal excitation with a characteristic lifetime [30]. If the APD is biased above breakdown before the traps have fully emptied, a trapped carrier can be used to initiate another avalanche [31]. In the context of QKD, the afterpulses contributes to the background of coincidence events which can lead to an overestimation of the total count rate and coincidence events. This eventually worsens the Quantum Bit Error Rate (QBER) which can adversely affect security.

Lengthening the dead time of the APD will ensure that the depopulation of traps happens before the APD is biased above breakdown, thus will not affect the actual count rate. However, a long dead time limits the maximum count rate and can distort the photocount statistics which degrades the APD performance [32]. The dead time of Si APDs is usually a few times more than that of InGaAs APDs, depending on the capacitance in the diode. The capacitance of Si APDs is in order of a few picofarad, whereas that of InGaAs APDs is less than 1 picofarad. Assuming R_B of 390 k Ω , the dead time of Si APDs would be a few microseconds, and for InGaAs APDs would be less than a microsecond.

Other methods to achieve quenching include active quenching, or operating the APD in gated mode. Active quenching is achieved when a fast discriminator senses the steep leading edge of the avalanche current across a resistor and provides a digital output pulse, synchronous with the photon arrival time. The circuit then quickly reduces the reverse bias to below breakdown voltage, and then raises the reverse bias to above the breakdown voltage for the next photodetection. Gated mode is achieved by periodically turning *on* (raise reverse bias above breakdown voltage) and *off* (lower reverse bias to below breakdown voltage) the APD, such that the APD only detects when there is incident optical light.

2.1.2 Pulse Discrimination and photon counting



Figure 5: Illustration of the setup used to process the APD pulse. The trigger level on the discriminator card is set slightly above the noise. A USBcounter is used as the counting unit, with counting period typically set at one second.

As mentioned in Section 2.1, a macroscopic pulse is produced as a result of the avalanche effect. This analog pulse from the APD is then sent into discriminator card which filters away pulses below a set reference voltage and converts pulses above a set reference voltage into a digital NIM² pulse. The NIM pulse is then sent to a counter unit, which outputs the number of counts detected over a set period of time. The process is illustrated in Figure 5.

²NIM stands for Nuclear Instrumentation Module which defines mechanical and electrical specifications for electronics modules. It is used to achieve flexibility, interchange of instruments, reduced design effort, ease in updating and maintaining the instruments. NIM is chosen here over TTL (Transistor-Transistor Logic) for its fast logic.

2.2 Characteristics of APD

This section discusses some of the APD characteristics which we are interested in, and are typical indicators of its performance. The characteristics includes the breakdown voltage, pulseheight distribution, dark count rate, detection efficiency, and timing jitter.

2.2.1 Breakdown voltage

We define breakdown voltage (V_{BR}) as the point at which we first see pulses with height greater than that of the noise. To do so, the oscilloscope is triggered to a level above the noise (typically a few millivolts) and the reverse bias voltage supplied to the APD is slowly increased until a breakdown pulse (typically a few tens of millivolts) is seen on the oscilloscope.

A higher V_{BR} would essentially mean more complex electronic components are involved which might increase the cost of implementation. The V_{BR} of our APDs used in this thesis typically ranges between 60 to 80 V.

Typically, a Geiger mode APD is biased beyond its V_{BR} and breaks down whenever a photo-event excites an electron into the conduction band. The device will continue to break down until the bias voltage is lowered to below V_{BR} , thus quenching the avalanche as mentioned in Section 2.1.1. APDs are usually biased 1V to 5V above breakdown voltage, where

$$V_{BIAS} = V_{BR} + V_{OV} \tag{2}$$

for the overvoltage V_{OV} .

Higher V_{OV} creates a higher electric field across the multiplication region which improves the gain of the APD [33]. However, higher V_{OV} also increases the after-pulsing probability due to the deeper trapping of free charges, and also increases the level of noise (dark counts).

2.2.2 Pulse height

The pulse height of an APD output signal is a representation of its responsivity, which corresponds to the multiplication gain (G), where a higher gain produces a higher pulse height (amplitude). G is defined as the number of photoelectrons created per incident photon, and can be obtained from

$$G = \frac{1}{R_L e} \int_0^{\infty} V(t) dt \quad (3)$$

where $V(t)$ is the amplitude of the pulse in Volts, and R_L is the load resistor of the passive quenching circuit as shown in Figure 4.

The gain must be high enough to deem useful. A higher gain would simply mean easier detection of the avalanche, while a low gain will not create any measurable output signal from the APD. Typically, the pulse height of a Si APD is in order of 100 mV, while that of an InGaAs APD is lower, in the order of 10 mV. From Equation 3, increasing the bias voltage sent to the APD would increase the pulse height of the APD thus improving the gain.

The pulse height is measured from the bottom to the top of the pulse as seen on the oscilloscope and illustrated in Figure 6. The measurements are histogrammed as shown in Figure 7. Apart from providing information on the pulse height trend, the histogram also serves as a reference to the trigger level we should set on the discriminator card. The trigger level should be set at the start of the rising edge of the peak, such that it filters away the pulse height of the noise.

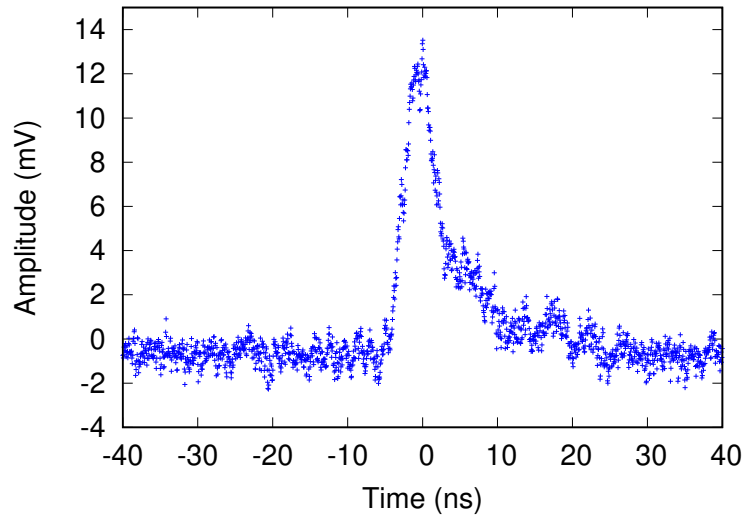


Figure 6: A typical analog pulse from an APD.

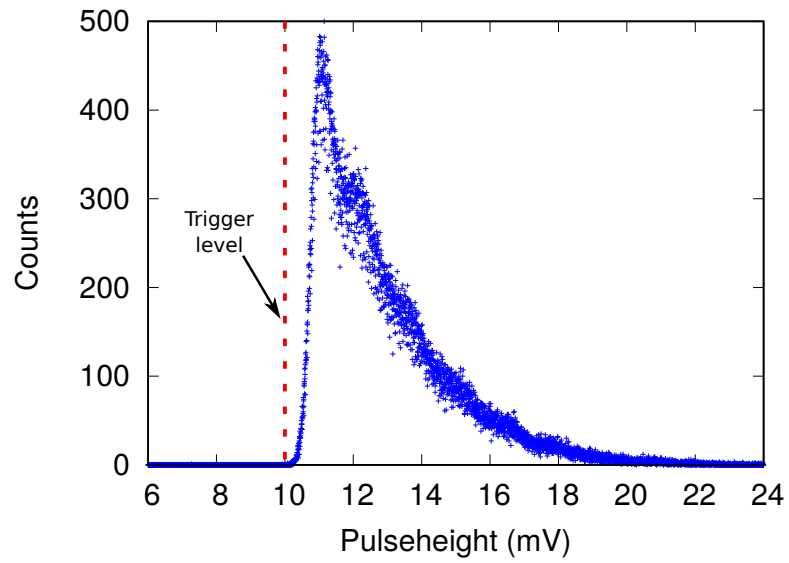


Figure 7: An example of a histogram of an APD pulse-height.

2.2.3 Dark count rate

Dark counts are unwanted pulses and are registered even when there is no light incident. Primary dark counts are the result of thermal energy exciting electrons and triggering avalanches as if they were real photon events [34], while secondary dark counts are created due to afterpulsing effects. The dark count rate also varies with the material used for the detector. Detectors for telecommunication wavelengths are typically based on germanium and InGaAs/InP. These materials do suffer from high levels of impurities due to the crystal growth process.

That said, APDs should be operated at lower temperatures so as to reduce dark counts caused by thermal excitations. However, too low a temperature might lead to higher afterpulsing probability because cooling slows the rate at which the traps release the charge carriers [35].

The dark count rate is easily measured by blocking the detector active area. In the context of QKD, it is important to choose an APD with low dark count rate because high dark count can lead to high QBER which would have adverse impact on the key rate and range of the QKD system.

2.2.4 Detection Efficiency

Detection efficiency is defined as the overall probability of registering a count if a photon arrives at the detector, factoring in the coupling efficiency ($\eta_{coupling}$) and quantum efficiency (η_{QE}) of the detector itself. Hence, η_{QE} is the efficiency with which photons are absorbed to create the electron-hole pairs. The total detection efficiency is given by

$$\eta = \eta_{coupling} \cdot \eta_{QE} . \tag{4}$$

It is important to find out this value because measurements which incorporate an APD will have measured efficiency that is limited by the losses in the APDs used. That said, in most applications, such as QKD and Light Detection And Ranging (LIDAR), a high detection efficiency is definitely desirable, however, it is not the only practical consideration. Here, we show two techniques to measure the detection efficiency.

A. Calibrated light source technique

This measurement involves measuring a light source with a calibrated photodiode and then attenuating the output down to single photon level to determine the number of photons. The setup is shown in Figure 8.

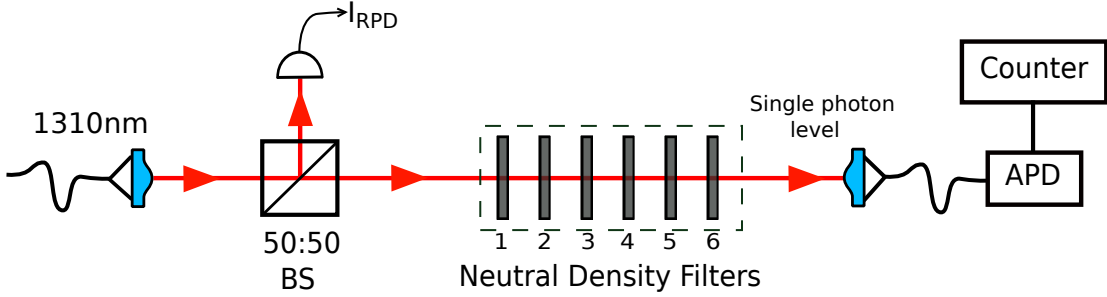


Figure 8: Setup for efficiency measurement. A 1310nm pulsed laser (5 mW) is split through a 50/50 beam splitter before being attenuated through a series of neutral density filters (90 dB) to transmit light at single photon level (11 nW) to the APD. The power of the light source after the beam splitter is measured by a calibrated Germanium photodiode (Thorlabs FDG03).

It is important to ensure that the fibre used have core size that match when connecting different fibres; for example, multi-mode fibre should not be coupled to single-mode fibre for it will lead to high losses. Calibration of the losses in the optical components is also done before proceeding with the measurement.

Beam-splitter The APD is initially substituted with another calibrated high gain germanium photodiode (we denote as CPD) and the beam splitting ratio R is determined by comparing the current readings detected by the two photodiodes,

$$R = \frac{I_{CPD}}{I_{RPD}}. \quad (5)$$

Neutral Density Filter (NDF) The attenuation of the NDF is determined by the ratio of the photodiode readings. The NDF used are anti reflection (AR) coated to minimise reflection from each filter surface. By individually inserting the NDF, the transmission factor (T_n) of the beam after passing through each filter can be determined by

$$T_n = \frac{R'}{R}, \quad (6)$$

where R' is the new splitting ratio measured by the CPD after inserting a single NDF.

Transmission factor The total transmission factor (T) of all the NDF is just a multiplication of all the respective T_n ,

$$T = \prod_{n=1}^6 T_n. \quad (7)$$

Incident light With all the NDF mounted as shown in Figure 8, the results between the APD and RPD are then compared to deduce the detection efficiency. Before initiating the measurement, the fibre coupling is optimised again to compensate for any beam deviation due to the insertion of NDF. With the values of R , T , I_{RPD} , and the sensitivity (s) of the RPD, the power incident onto the APD (P_{in}) can be determined by

$$P_{in} = \frac{I}{s}(R)T. \quad (8)$$

Subsequently, the number of photons incident onto the APD per second ($count_{in}$) is given by

$$count_{in} = \frac{P_{in}}{h\nu}. \quad (9)$$

The measurement is then repeated for a dark count measurement at the respective APD operating conditions. Finally, with the number of counts and dark counts detected ($count_{out}$), the efficiency of the APD can be calculated:

$$\text{Efficiency} = \frac{\text{count}_{\text{out}} - \text{count}_{\text{dark}}}{\text{count}_{\text{in}}} \quad (10)$$

B. Correlated photon technique

The correlated photon technique for the measurement of detector efficiency involves using a source of correlated photons to establish the pairs-singles ratio. The setup is as shown in Figure 9.

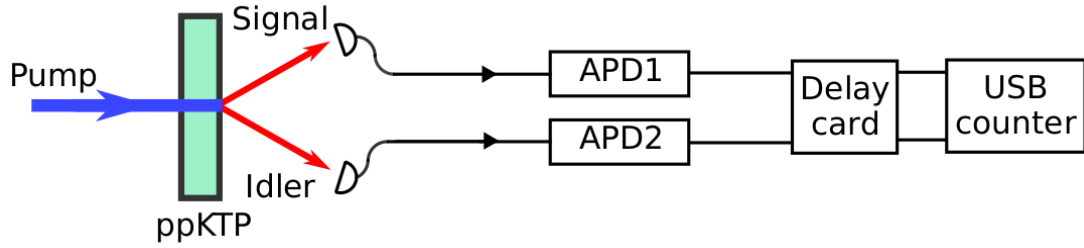


Figure 9: Setup for measuring pairs-singles ratio. The pump photon is at a wavelength of 658nm, and the signal and idler photons obtained are centered at about 1316nm. A counter is used to measure the output counts of the APD.

This technique does not require any attenuation of light nor calibration of optical components. It relies on the process of optical parametric downconversion where a high-energy photon in a suitable non-linear crystal can spontaneously decay into two lower energy photons at the same time. The two photons have combined energies and momenta equal to the energy and momentum of the original photon, frequency phase-matched, and have correlated polarizations. Detection of a signal photon indicates that its twin must exist.

The photon pairs are then sent to two APDs, where the singles are detected by the respective APDs, and then subsequently sent to a coincidence stage. Knowing the singles rate of the APDs and their corresponding coincidence rate will allow us to obtain the detection efficiency of the respective APDs. We first denote the following:

$$\begin{aligned}
S_1 &= \text{Singles rate of APD1} \\
S_2 &= \text{Singles rate of APD2} \\
S_1^{dark} &= \text{Dark count rate of APD1} \\
S_2^{dark} &= \text{Dark count rate of APD2} \\
S_T &= \text{Number of incident photon pairs} \\
C &= \text{Coincidence rate of APD1 and APD2} \\
\eta_1 &= \text{Detection efficiency of APD1} \\
\eta_2 &= \text{Detection efficiency of APD2} \\
t_c &= \text{Coincidence time window}
\end{aligned}$$

The respective singles rate is determined by the number of incident down-converted photons, taking into account the detection efficiency of the APDs as well as the corresponding dark count rates, where:

$$\begin{aligned}
S_1 &= S_T \eta_1 + S_1^{dark} \\
S_2 &= S_T \eta_2 + S_2^{dark}
\end{aligned} \tag{11}$$

The coincidence rate of the two APDs, taking into account the accidental rate, is simply:

$$C = S_T \eta_1 \eta_2 - S_1 S_2 t_c \tag{12}$$

However, since t_c is set to 2 ns throughout our measurements, we expect the accidental rate to be very small compared to the coincidence rate. Therefore, substituting the above equations, we obtain:

$$\begin{aligned}
C &= S_T \left(\frac{S_1 - S_1^{dark}}{S_T} \right) \eta_2 \\
\eta_2 &= \frac{C}{S_1 - S_1^{dark}} \\
\eta_1 &= \frac{C}{S_2 - S_2^{dark}}
\end{aligned} \tag{13}$$

However, this technique only gives the overall efficiency of the test detector and collection optics, and thus represents a lower bound to the detection efficiency.

Calibrating the detection efficiency of a APD can simplify future characterisa-

tion where the calibrated APD can be used to do direct comparison with another APD.

2.2.5 Timing Jitter

In many experimental methods such as time-resolved spectroscopy [36] or quantum communications [37], precise timing of photon arrival is essential. Timing jitter is defined as the statistical fluctuations of the time interval between the arrival of a photon at the detector and the output electrical pulse from the detector [38].

The avalanche pulse of the APD is correlated with the arrival time of the photon that generates the free electron-hole pair. However, due to various physical effects, the time at which the avalanche is produced and the true arrival time of the photon at the APD is not constant. This can stem from the differences in the transit times of photoexcited charge carriers resulting from differences in the location of the photon absorption.

The setup for measuring timing jitter of an APD is shown in Figure 10. The correlated photon pair source is chosen for this measurement for it has negligible timing jitter as compared to the pulsed laser source. To measure timing jitter accurately, it is important that we ensure that the dominant jitter is solely due to that of the detector, and not any other external factors.

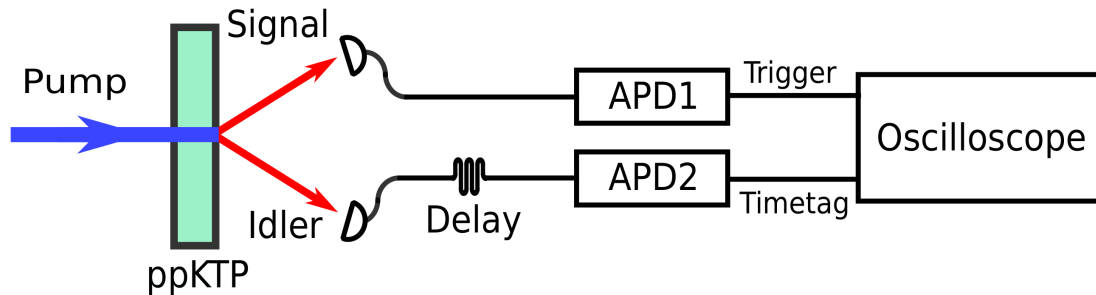


Figure 10: Setup for jitter measurement. The same correlated photon pair source as mentioned in Figure 9 is used. The oscilloscope triggers on the signal from APD1 and timetag on the signal from APD2.

The timing jitter is measured with two APDs connected to the pair source, with

the output of the respective APDs connected to the oscilloscope. One of APDs is delayed by using a longer cable (1 meter of cable gives an additional delay of approximately 5ns) such that the oscilloscope can measure a non-zero time coincidence. The oscilloscope is set to qualify on one APD signal, and to trigger on the other APD signal, then measures the time delay between the two signals at their leading edges. To reduce the dead time between acquisitions, the time between the qualifier and trigger is set to below 20 ns, in consideration of the path length difference (due to different cable length). To speed up the data-taking process and also further reduce the dead time between triggers, the oscilloscope is set to “sequence mode” where multiple measurements are taken before display.

In this characterisation, timing jitter of the light sources and electronics (electronic discrimination of the edge) can also contribute to the overall timing jitter of the APD. However, the dominant contribution of timing jitter is from the APD itself.

A typical photon-timing distribution is shown in Figure 11.

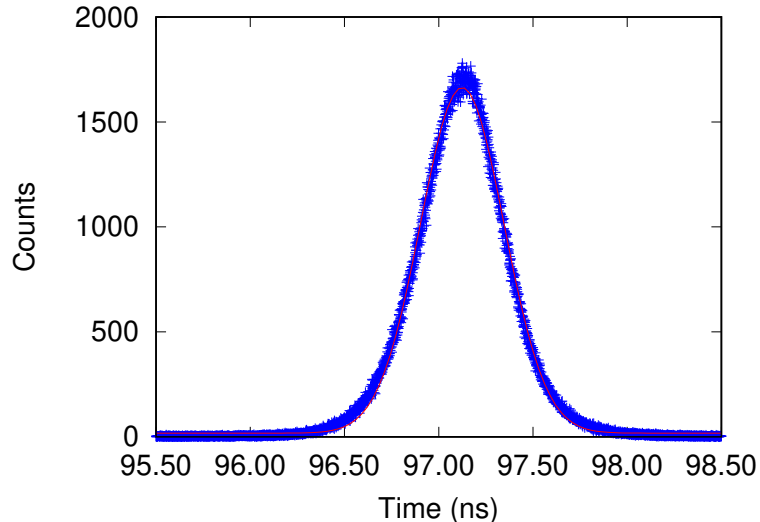


Figure 11: Histogram of the time difference in photon arrival measured between two APDs.

We assume that the distribution of the time difference follows a Gaussian distribution as in equation 14, where a is the amplitude of the peak, b is the full width at half maximum (FWHM) of the peak, c center of the peak, and k is the fitting

parameter that represents background noise:

$$f(x) = k + ae^{-\frac{(x-c)^2}{2b^2}} \quad (14)$$

We also assume that the timing jitter of the APDs are independent values, where one APD does not depend on that of the other. Since the histogram of the time delay between the two signals is a distribution of the time difference of the two APD signals, the histogram plot is a convolution of the timing jitter of 2 APDs where:

$$\begin{aligned} \delta_{APD1} &= \text{Timing jitter of APD1} \\ \delta_{APD2} &= \text{Timing jitter of APD2} \\ \delta_{total} &= \text{FWHM} \end{aligned} \quad (15)$$

The square of FWHM is thus the uncertainty of the sum of two independent uncertainty (adding in quadrature), whereby:

$$\delta_{APD1}^2 + \delta_{APD2}^2 = \delta_{total}^2 \quad (16)$$

If we assume both APDs have the same timing jitter, where $\delta_{APD1} = \delta_{APD2} = \delta_{APD}$, then:

$$\begin{aligned} 2\delta_{APD}^2 &= \delta_{total}^2 \\ \delta_{APD} &= \sqrt{\frac{\delta_{total}^2}{2}} \end{aligned} \quad (17)$$

However, if we expect the timing jitter of the two APDs to be different, then we fit the data to a “double Gaussian” equation, where:

$$f(x) = k + a_1 \exp\left(\frac{-(x-b_1)}{c_1}\right)^2 + a_2 \exp\left(\frac{-(x-b_2)}{c_2}\right)^2 \quad (18)$$

If we know the jitter information of one of the two APD, we can fix the parameters for one of the two Gaussian, and fit the rest of the parameters to get the jitter information of the second APD.

2.3 APD for QKD

The credibility of a QKD system depends on the quantum bit error rate (QBER). The QBER is defined as the ratio of wrong bits to the total number of bits received. It can be expressed as a sum of error rate contributed by different factors, the simplest case would briefly be:

$$QBER = QBER_{opt} + QBER_{det}, \quad (19)$$

where $QBER_{opt}$ is the error contributed by the optical quality of the setup, and $QBER_{det}$ is the error contributed by detector dark counts.

In fibre-based QKD, $QBER_{opt}$ increases with distance; since bit rate reduces with longer distance while dark count rate of the detector is independent of distance. Improving the QBER would require a detector which has dark count rate as low as possible and also high detection efficiency to increase bit rate.

In general, we expect an ideal detector to fulfil the following requirements:

1. The detection efficiency should be high over a large spectral range.
2. The dark count rate (noise) should be small.
3. The timing jitter should be small to ensure good timing resolution.
4. The dead time should be short to allow high count rates (bit rate).

However, it turns out that it is impossible to fulfil all the above criteria at the same time; one is better at the expense of another. Increasing bias voltage can improve detection efficiency and lower timing jitter, however, at the cost of an increase in noise. Operating the APD at a lower temperature can reduce dark count rate, but increases the afterpulsing probability. Lengthening the dead time of the APD can lower the afterpulsing probability, however, there is a tradeoff between high count rates and low afterpulses.

Therefore, the aim is to investigate the performance of various APDs and ultimately select one which best meets the above requirements. Knowing the APD performance allows one to find a suitable operational setting such that it can behave to the expectations of its application. The choice of the APD also needs

to be economically viable because ultimately, a deployed large scale QKD system would require many APDs, thus cost and functionality would become a concern.

3 Characterisation of APD

In this section, we examine the InGaAs APDs from four different manufacturers, namely ID Quantique, Laser Components, Princeton Lightwave, and Renesas. InGaAs APDs were chosen over other materials such as Silicon or Germanium for it has a broad and higher spectral responsivity at the telecommunication bands (1310 nm or 1550 nm) where optical fibers have the lowest loss.

The InGaAs APDs include commercial detection modules which are APD diodes housed in a huge heat sink with in-built detection circuitry, and also bare diodes which would require appropriate external detection circuitry and cooling. Commercial modules are often convenient, user-friendly, and more stable but most of the time costly (>\$20,000 per module). Moreover, there are not many InGaAs APDs in the current market, which makes these modules all the more expensive. Therefore, it is important to explore alternatives such as the bare diodes which are not only cheaper (can range from \$500 to \$10,000 per diode), but also allow more flexibility in the packaging and designing of the overall APD unit.

The characterisation would begin with commercial detection modules, where the results would serve as a reference and benchmark to what we should expect from the performance of the bare diodes.

3.1 Characterisation of commercial modules

3.1.1 ID Quantique ID220-FR

The ID220-FR, as shown in Figure 12, is an InGaAs APD based single-photon counting module which encompasses an internally cooled InGaAs/InP diode and associated circuitry in a relatively large heatsink.



Figure 12: ID Quantique ID220-FR module. The APD is free-running (FR) which means it is not gated, and is usually used in cases when the arrival time of the photons is not precisely known. A gated mode will allow rapid quenching of the avalanche current, however, this APD is designed for providing a fast avalanche quenching even in FR mode.

The only available settings are the detection probability level and the dead time which can be done through a simple USB interface on the module. The module can be set to operate at three detection probability levels of 10 %, 15 % and 20 % which represents the different level of reverse bias voltage supplied, and not the real detection probability of the APD. The dead time of the module can also be set between $1 \mu\text{s}$ and $25 \mu\text{s}$. The higher the detection probability level, the higher the reverse bias voltage sent to the APD. A standard FC/PC connector is provided as an optical input and the output (TTL signal pulse with 100 ns width) is read through an SMA connector.

Dark count rate

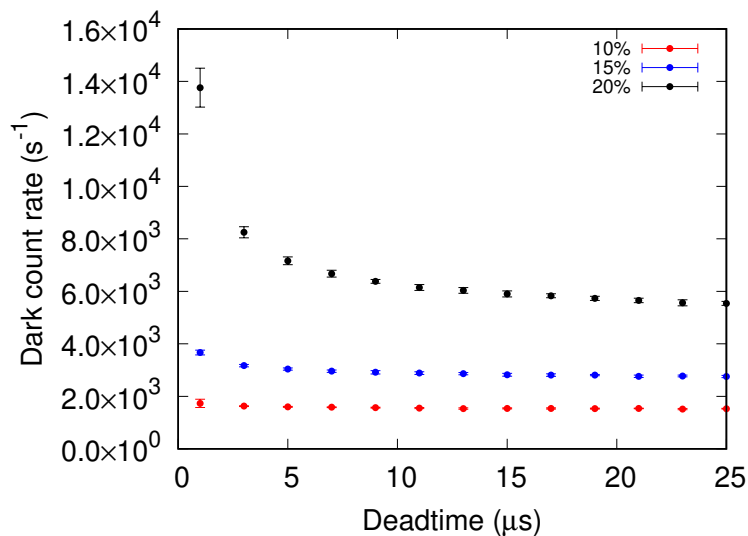
The dark count rate is characterised as a function of the detection probability and dead time setting (the temperature of the APD is non-adjustable on the user end). The results for two individual ID220 modules are shown in Figure 13.

The results show that, for both modules, dark count rate generally increases with higher detection probability setting (higher reverse bias voltage), which agree with results reported previously [33, 39]. This is due to the fact that a higher reverse bias voltage strengthens the electric field across the depletion region, thus leading to the generation of more breakdown events.

It is also observed that the dark count rate is not affected by dead time setting beyond $5 \mu\text{s}$ however, increases with dead time setting below $5 \mu\text{s}$. This could be due to afterpulsing, where trapped charges have a lifetime longer than the dead time setting. The trapped charges end up being released during the non-conducting state of the APD, where the APD is ready for the next photodetection event; this contributes to a higher dark count rate. Setting the ID220 at dead time beyond $5 \mu\text{s}$ would ensure that the dark count rate stays relatively low.

Comparing the results from two individual ID220 modules, it is surprising that the two modules, which are fabricated in separate batches but have the same design parameters, can exhibit dark count rate that differ by almost a factor of 2. At detection probability of 20% and $10 \mu\text{s}$ dead time, Module 2 agrees better with the datasheet value of 5000 s^{-1} dark count rate. This shows that characterisation of each and every individual APD is important, and one should only take the values quoted on the data sheet as a reference.

(a) Module 1



(b) Module 2

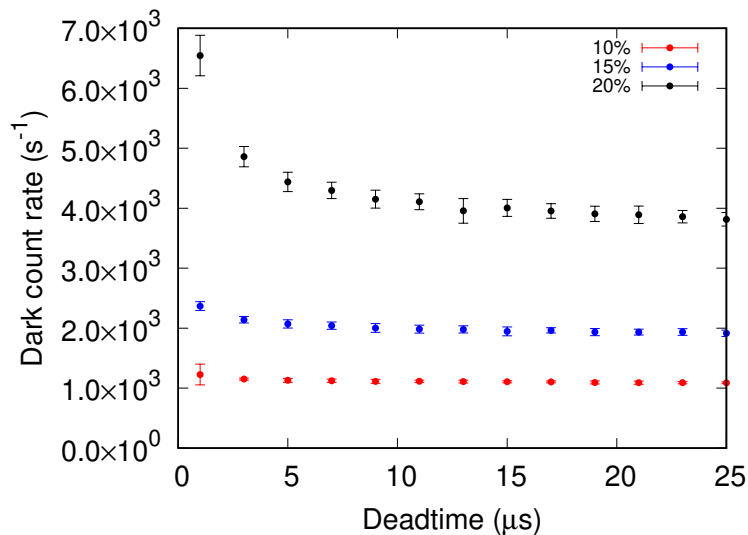


Figure 13: Dark count rate as a function of the detection probability setting and dead time setting. The detection probability and dead time are set at 10 %, 15 %, 20 %, and 1 μs to 25 μs in step of 2 μs , respectively. At each setting, the detection events were integrated for a total of 10 minutes — 60 measurements each with 10s integration time. This is due to the maximum integration time of 10s of the counter.

Detection Efficiency

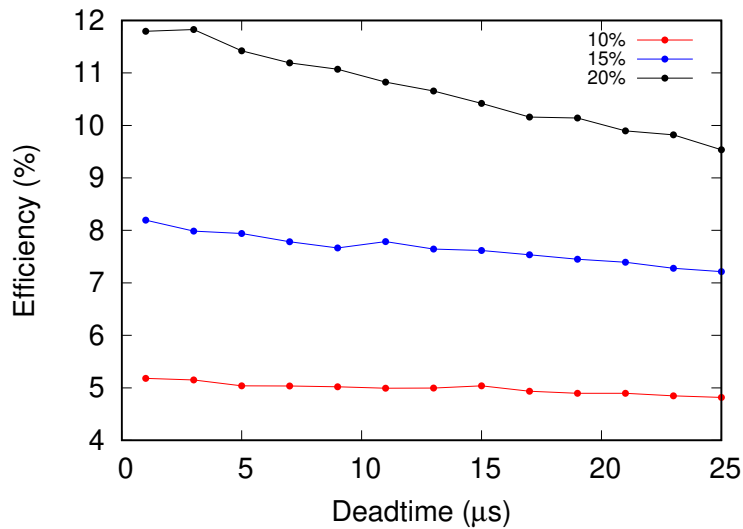
The characterisation of detection efficiencies of the two ID220 was first done using a pair source as mentioned in Section 2.2.4 to establish the pairs-singles ratio giving a lower bound to the efficiencies, before continuing with the measurement through a calibrated light source to establish the absolute efficiencies.

For the correlated photon technique, the measurement involved one APD set at a detection probability of 20 % ($V_{\text{BIAS}} = 84 \text{ V}$) and dead time of $1 \mu\text{s}$, while varying both settings for the other APD. The singles from both modules are recorded and the coincidence between them is also recorded within a time window of 5 ns. For the calibrated light source technique, the measurement involved only one APD at a time, and the settings are systematically varied. Dark count rate is accounted for in both results, where the dark count is subtracted from the respective detected count. Figure 14 and 15 show the results for both modules using both techniques respectively.

Both results show that detection efficiency increases with higher detection probability setting (higher reverse bias voltage), similar to the behaviour of its dark count rate. However, both results differ when comparing detection efficiency against dead time. In Figure 14, detection efficiency reduces with longer dead time, and the effect is even more apparent if the reverse bias is higher. On the other hand, in Figure 15, detection efficiency is observed to be relatively constant for all dead time values, except for a short dip at the highest reverse bias with shortest dead time setting.

The reduction in detection efficiency as shown in Figure 14 could be due to saturation of the APD, where the number of incident photons is too high. This is because a higher dead time would imply more incident photons not getting absorbed, thus when fewer photons are detected with the same amount of incident photons, detection efficiency will reduce.

(a) Module 1



(b) Module 2

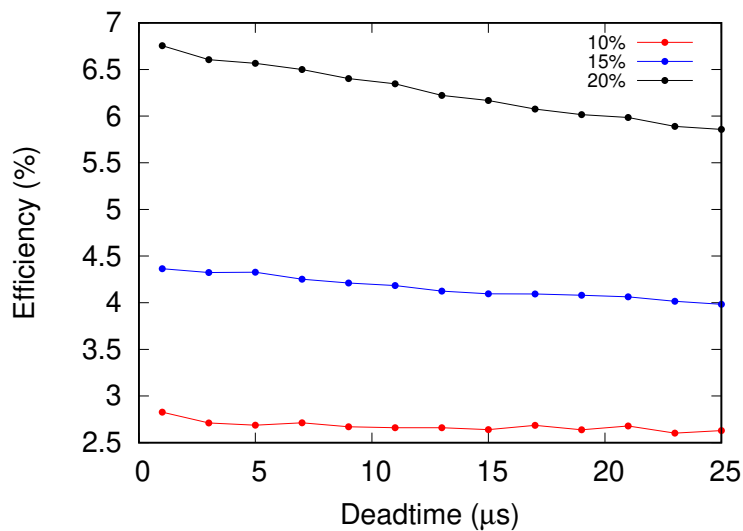
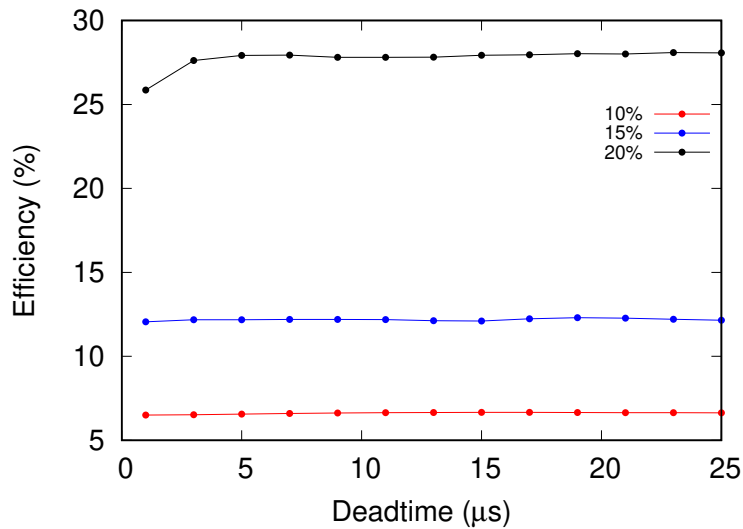


Figure 14: Detection efficiency as a function of the detection probability setting and dead time setting, obtained with the correlated photon technique. At each setting, the detection events were integrated for a total of 10 minutes — 60 measurements each with 10s integration time.

(a) Module 1



(b) Module 2

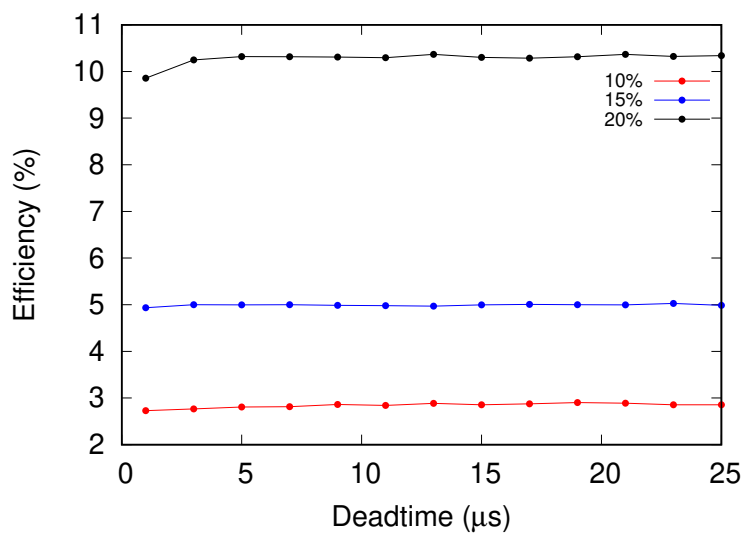


Figure 15: Detection efficiency as a function of the detection probability setting and dead time setting, obtained with the light attenuation technique. At each setting, the detection events were integrated for a total of 10 minutes — 60 measurements each with 10 s integration time.

Timing jitter

The time delay between the two ID220 modules is measured with one of the detectors set at a deadtime setting of $2\ \mu\text{s}$ and detection probability settings of 20 %, with the other detector at varied settings. Using the method as mentioned in section 2.2.5, we can deduce from the measured FWHM of the histogram, the timing jitter of the APD.

Figure 16 shows the results obtained at three different detection probability settings for both modules as a function of the deadtime setting. At detection probability of 10 %, 15 %, 20 %, the average timing jitter values for Module 1 are $(283.0 \pm 2.1)\ \text{ps}$, $(156.2 \pm 0.6)\ \text{ps}$, $(93.2 \pm 0.3)\ \text{ps}$ respectively, and for Module 2 are $(319.0 \pm 4.5)\ \text{ps}$, $(167.5 \pm 0.5)\ \text{ps}$, $(93.4 \pm 0.4)\ \text{ps}$ respectively.

For both modules, it is observed that timing jitter does not vary with the dead time of the APD. This is expected because there should be no output signal from the APD during its “unresponsive” period, thus lengthening the dead time will not have an impact on the timing jitter values. The results also show that the timing jitter is higher at lower detection probability (lower reverse bias voltage) setting. However, achieving low timing jitter by setting higher reverse bias poses a trade-off with dark count rate and afterpulsing probability. Both observations are also consistent with results reported elsewhere [39, 40, 41].

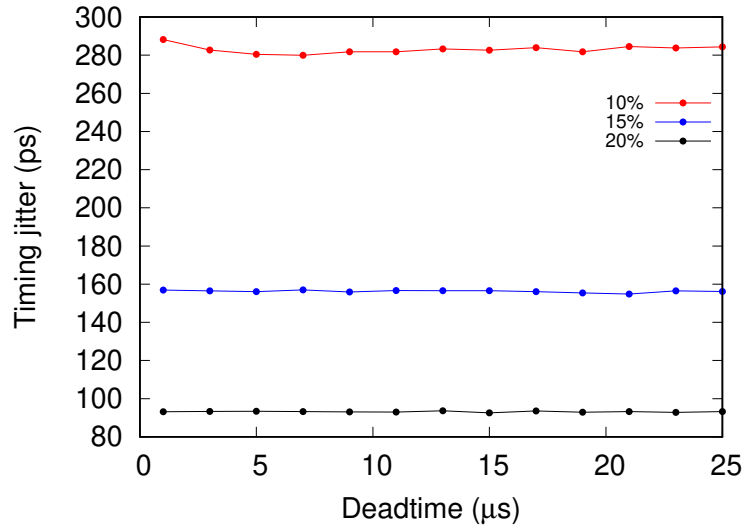
We also see that the two modules have slightly different timing jitter, which makes our initial assumption of both APDs having the same timing jitter not justified. A more rigorous approach would be to initiate a triangle measurement to establish independent jitter measurements for three APDs, where time correlation measurements are done for combinations of the three APDs. Their independent timing jitter is then obtained by solving the three simultaneous equations as follows:

$$\delta_{APD1}^2 + \delta_{APD2}^2 = C_1 \quad \delta_{APD2}^2 + \delta_{APD3}^2 = C_2 \quad \delta_{APD3}^2 + \delta_{APD1}^2 = C_3$$

Thus,

$$\delta_{APD1} = \sqrt{\frac{C_1 + C_3 - C_2}{2}} \quad \delta_{APD2} = \sqrt{\frac{C_1 + C_2 - C_3}{2}} \quad \delta_{APD3} = \sqrt{\frac{C_2 + C_3 - C_1}{2}}$$

(a) Module 1



(b) Module 2

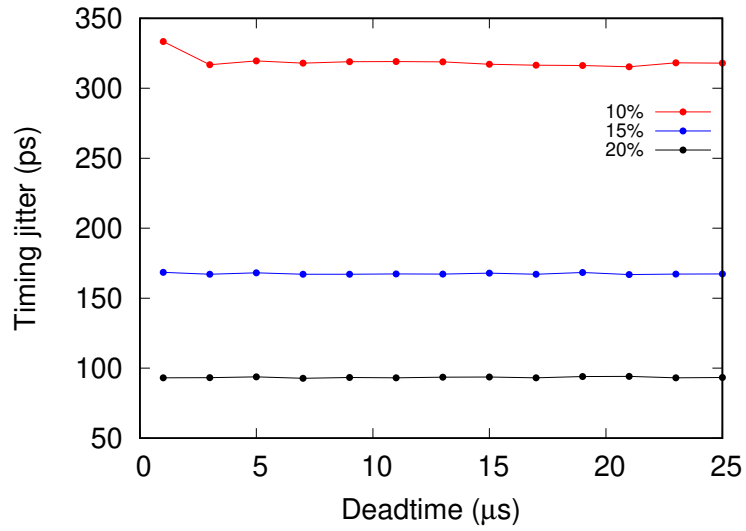


Figure 16: Timing jitter as a function of deadtime setting at detection probability setting of 10 %, 15 %, and 20 %.

Summary for ID Quantique ID220

From the characterization of dark count rate, detection efficiency, and timing jitter, we can conclude that even identical detectors of the same brand and model can behave very differently. Therefore, it is important for characterisation to be done for each and every individual detector. The values provided by the datasheet should only be taken as a reference.

Characteristic	Module 1	Module 2	Data sheet
Dark count rate (s^{-1})	7000	4500	5000
Detection efficiency (%)	27.5	10.2	20
Timing jitter (ps)	283	319	250

Table 1: Characteristics of ID Quantique, ID220.

3.1.2 Laser Components COUNT Q

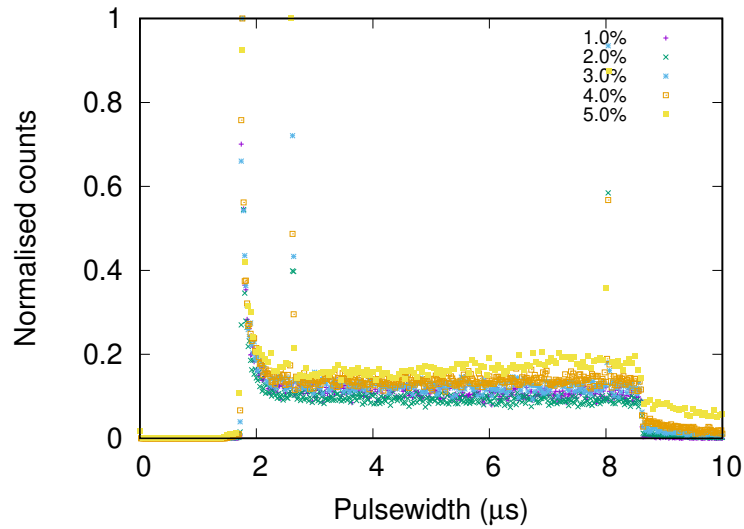
Laser Components COUNT Q is an InGaAs APD based single-photon counting module which encompasses an internally cooled InGaAs/InP diode and associated electronics in a relatively large heatsink. Incoming photons generate corresponding electrical pulses which are converted to digital pulses and conveniently read out at the TTL output. The FC connector is provided as an optical input, and the APD can be set to operate at detection probabilities of 0 to 20 % and dead time of 0.1 to 5 μ s.

The pulsewidth of the TTL pulse is an indication of the dead time of the APD; the longer the pulsewidth, the longer the deadtime of the APD. The histogram of the pulsewidth measured as a function of detection probability and dead time settings is shown in Figure 17. The measurement was done in dark conditions.

In Figure 17a, the pulsewidth does not seem to be affected by detection probability setting (reverse bias voltage). However, a significant population represented by the long tail of the histogram suggests that there is a huge spread in the width of the TTL pulse. This implies a continuously changing dead time of the APD which conflicts with the deadtime setting of 2 μ s. Next, setting the detection probability at 1.0%, the pulsewidth was measured at different deadtime settings. It is observed that the minimum pulsewidth of each histogram coincides with the respective dead time setting, but the spread in pulsewidth was still apparent.

The implication of the huge spread (6 μ s) of the pulsewidth is a continuously changing APD dead time which would lead to extremely low and uncertain count rate. As a result, the APD would most likely to saturate when there is a long pulsewidth. This APD would only be useful when saturation did not occur, for instance, when the incident light level is extremely low (low incident photon count rate). The problem was not rectified at time of writing because it seems to be due to a “design bug” during the manufacturing of the APD. This reinforces the importance of characterisation of detectors prior to any applications.

(a) Histogram of pulsewidth against detection probability



(b) Histogram of pulsewidth against dead time

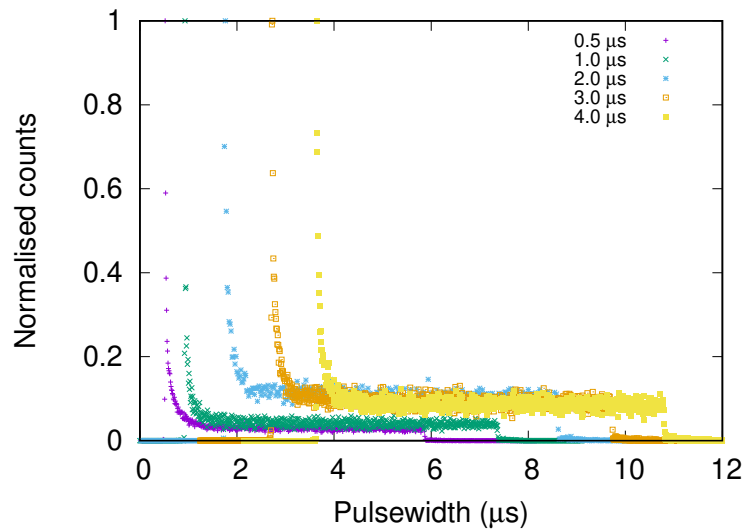


Figure 17: Histogram of pulsewidth as a function of detection probability and dead time, respectively. The detection probability was set to 1.0% for measurement against dead time, and the dead time was set to 2 μs for measurement against detection probability.

3.2 Characterisation of bare diodes

Unlike commercial modules, APD bare diodes have to be “packaged” and attached to an external detection circuitry for biasing, read-out, and temperature control. The typical measurement apparatus is shown in Figure 18. A high voltage supply is used to supply the reverse bias. The reverse bias voltage across the APD is measured by a multimeter. The APD breakdown pulses are sent to a simple discriminator which converts the analog output pulse into digital NIM pulses, and with a threshold set above the noise level to ensure no extraneous noise pickup. A counting unit then outputs the APD count.

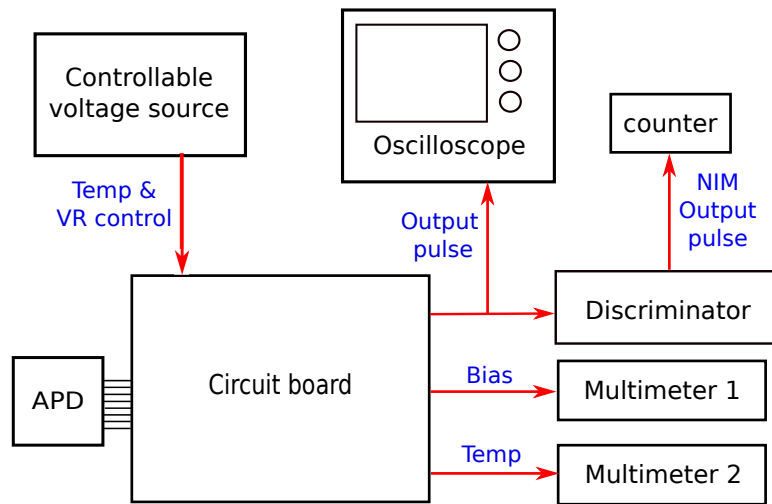


Figure 18: A schematic illustration of the apparatus used to operate the APD. The circuit board routes the high voltage supply, temperature control, and the read-out for the reverse bias voltage, temperature, and APD output pulse.

A simple detection circuitry is designed to adapt the diode to the APD testing kit. The circuitry includes a ballast resistor of $390\text{ k}\Omega$ to ensure good quenching for all overvoltages (0 to 2 V). The bare diode is either housed in or attached to a heatsink with thermal paste to allow good dissipation of heat.

3.2.1 Princeton Lightwave PGA-016u-1550TFT

The Princeton Lightwave PGA-016u-1550tft is an InGaAs APD in a fibre pigtailed TO-8 package with integrated TEC. It is designed specifically for the detection of single photons in the wavelength range from 0.9 to 1.6 μm .

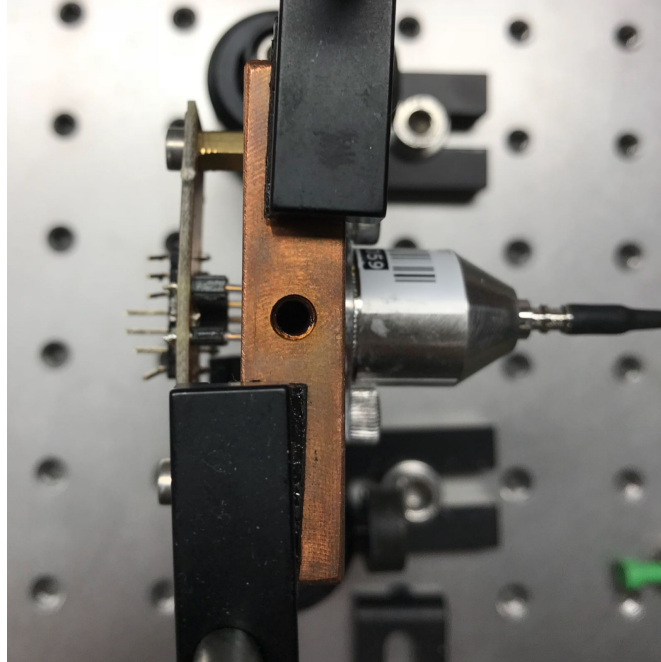


Figure 19: An assembled PGA-016u-1550TFT. The APD is attached to a copper heatsink and passively quenched with a ballast resistor of 390 k Ω .

The APD has an integrated TEC which is connected to a temperature controller of a laser driver (Stanford Research Systems LDC500), and the output connected to the oscilloscope or counting unit for output measurements. The lowest stable temperature attained with this configuration is -45°C with a breakdown voltage of 62.82 V.

Pulse height

The pulse height of the APD output pulse is characterised as a function of reverse bias voltage at temperature of $-40\text{ }^{\circ}\text{C}$ and $-45\text{ }^{\circ}\text{C}$ as shown in Figure 20.

It is observed that the peak of the histogram (typical pulse height) of the APD output signal increases with higher reverse bias voltage. This can be due to a higher electric field across the depletion region which causes stronger impact ionization that intensifies the avalanche multiplication process. The width of the histogram is also noticeably wider with higher reverse bias voltage, which implies larger uncertainty in the number of induced free charge carriers. However, this should not pose a problem as long as the discriminator is set to discriminate signals lower than the minimum pulseheight of the signal.

Comparing Figure 20a and 20b, the breakdown voltage (represented by the reverse bias of data in purple) is observed to be lower at colder temperature. The small peak in Figure 20b is suspected to be due to larger afterpulsing effects at a lower temperature.

The observations are consistent with other literatures [42, 43].

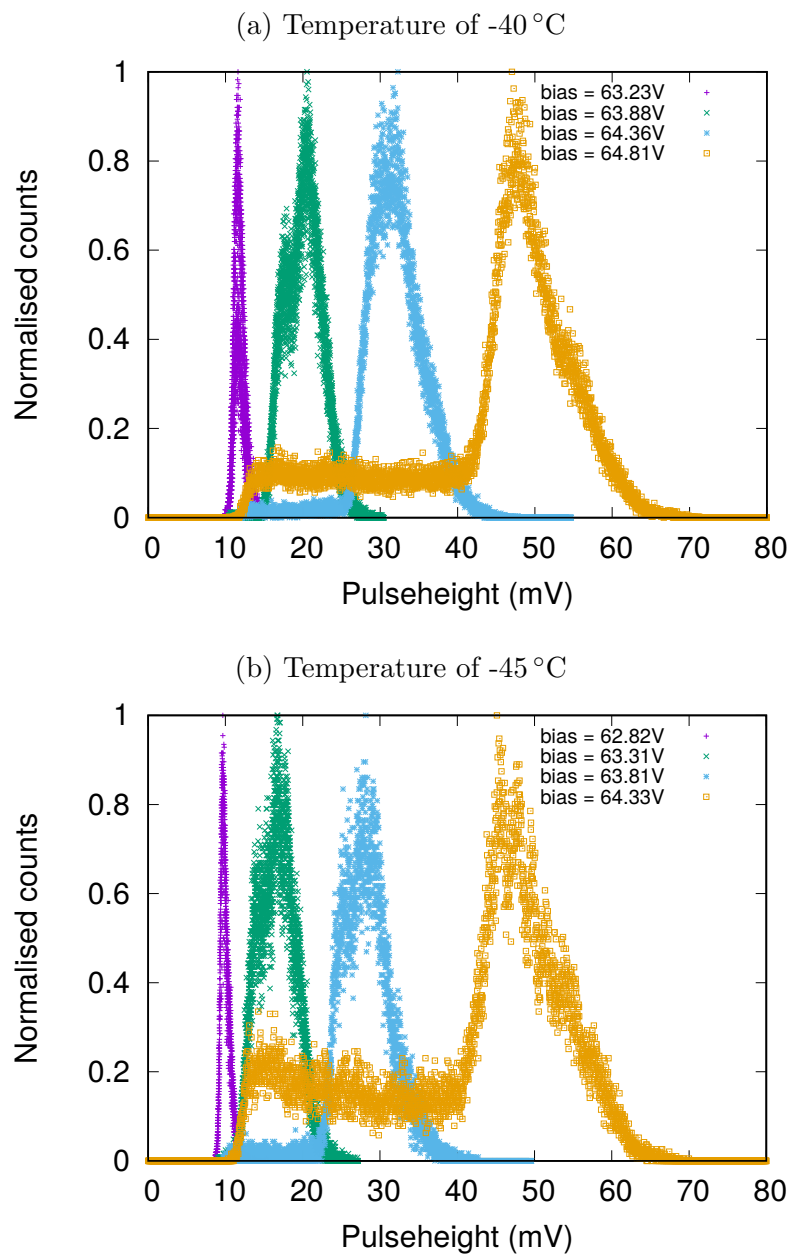


Figure 20: Histogram of pulse height at reverse bias voltages measured at two different temperatures. The trigger level on the oscilloscope was set to 7.8 mV.

Dark count rate

The dark count rate is measured as a function of reverse bias voltage at temperatures of -40°C and -45°C as shown in Figure 13.

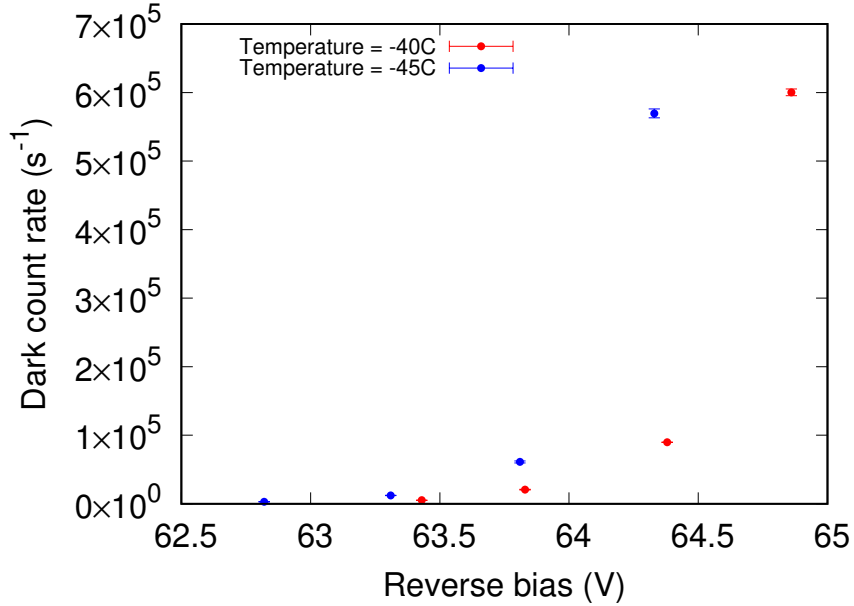


Figure 21: Dark count rate as a function of reverse bias voltage at temperatures of -40°C and -45°C . The reference level on the discriminator card was set to 9.4 mV . The detection events were integrated for a total of 10 minutes — 60 measurements each with 10 s integration time. This is due to the maximum integration time of 10 s of the USB-counter.

The results show that the dark count rate is higher with higher reverse bias voltage, similar to that of ID Quantique, ID220, measured previously. It is also observed that the dark count rate is reduced with lower temperature, which is what we expected since dark counts caused by thermal excitations are reduced at colder temperature. The lowest dark count rate attained at temperature of -40°C and -45°C is approximately 2900 s^{-1} and 2200 s^{-1} .

Detection Efficiency

The characterisation of detection efficiency was done using the light attenuation method as mentioned in Section 2.2.4. This is because we want to obtain the absolute detection efficiency instead of getting a number for the lower bound detection efficiency. The results for detection efficiency as a function of reverse bias voltage at temperatures of -40°C and -45°C is shown in Figure 22.

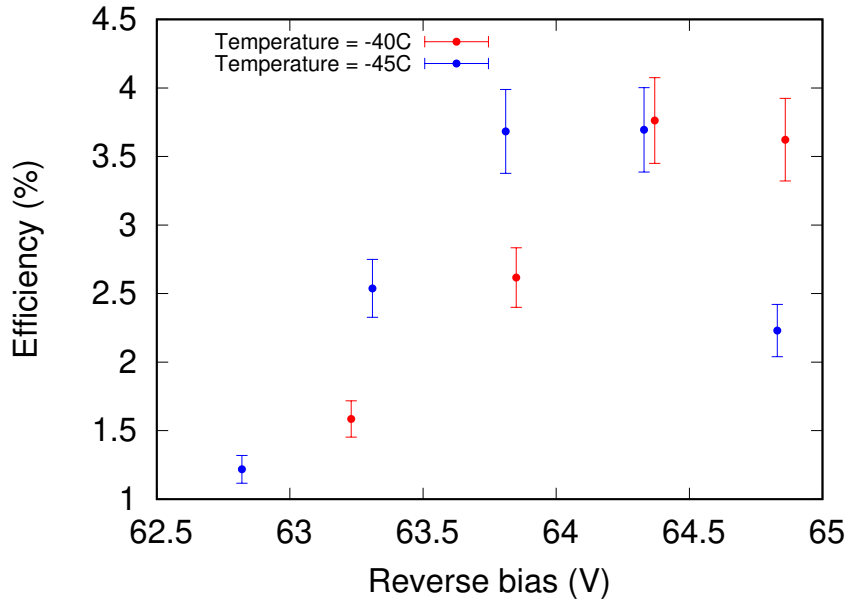


Figure 22: Detection efficiency as a function of reverse bias voltage at temperatures of -40°C and -45°C .

We observe similar variation of detection efficiency with reverse bias voltage at both temperatures. The detection efficiency reaches a maximum of approximately 3.8% before it decreases again. This behaviour matches with the characterisation found in other literature [39, 43].

Summary for Princeton Lightwave PGA-016u-1550TFT

The APD, at its lowest attainable temperature of -45°C , gives a dark count rate of approximately 2200s^{-1} , which is encouraging as it shows that low dark count rate is attainable with just Peltier cooling. However, despite a low dark count rate, its detection efficiency is too low to be useful.

3.2.2 Renesas NR8360JP-BC

The Renesas NR8360JP-BC is a fibre-pigtailed APD which is manufactured for operation in linear mode. Each diode cost about \$2100; more than three times cheaper than a Princeton Lightwave PGA-016u-1550TFT diode which costs about \$7200. Since linear mode and Geiger mode differs by the bias voltage applied, we attempt to bias this APD beyond its breakdown voltage to see if it exhibits behaviour of single photon detection.



Figure 23: A fully assembled Renesas NR8360JP-BC with an adapter board, and its flange in contact with the blue heatsink-fan with thermal paste in between for heat dissipation purposes. The APD is passively quenched by a ballast resistor of $390\text{ k}\Omega$.

The APD is packaged in a case together with an integrated TEC as shown in Figure 23. The TEC is then connected to a temperature control of a laser driver, and the output connected to the oscilloscope or counter for output measurements. The lowest stable temperature attained with this configuration is -10°C . The breakdown voltage was found to be 64.5 V at -10°C , as compared to 68.6 V at surrounding temperature of 22°C .

Pulse height

The histograms of pulse height at varying bias voltages are shown in Figure 24.

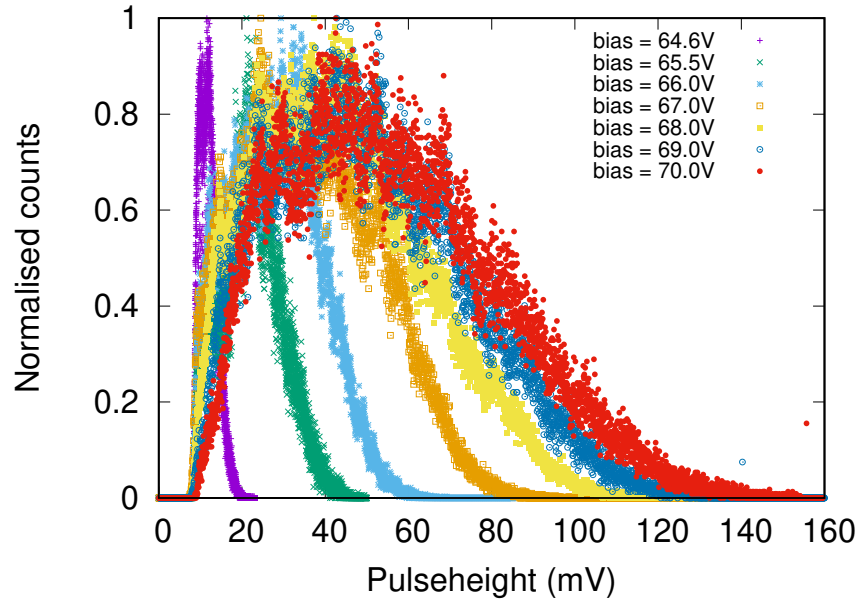


Figure 24: Histogram of pulseheight at varying bias voltages of NR8360JP-BC. The trigger level on the oscilloscope was set to 6 mV.

The APD was cooled to -10°C , which is the lowest temperature attainable in this configuration. The width of the histogram increases with increasing reverse bias voltage, which implies that the output signal is noisier with a higher electric field.

Dark count rate

At the same temperature of -10°C , the dark counts are measured at different bias voltages and the results are shown in Figure 25.

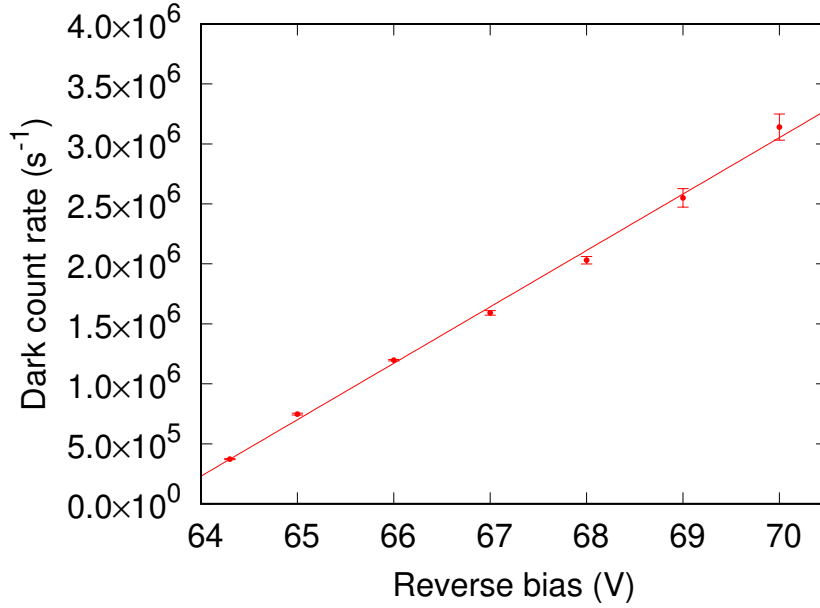


Figure 25: Dark count rate against reverse bias voltages NR8360JP-BC. The reference level on the discriminator card was set to 9 mV. The dark count rate is obtained by measuring the dark counts at every second for a total of 5 minutes and averaging. The error bar shown represents the standard deviation of the data points.

The dark count rate seemed too high (more than $100,000 \text{ s}^{-1}$) even at its lowest temperature. We suspect that the high dark count rate is due to insufficient cooling of the APD, thus we proceed to characterise the other version of this APD with no integrated TEC such that we can adopt our own cooling method to lower the temperature.

3.2.3 Renesas NR8800FS-CB

The NEC NR8800FS-CB is the “naked-diode” version of the NEC NR8360JP-BC, where there is no integrated TEC. Each diode costs about \$500, the cheapest among our inventory of APDs.

APD cooling solutions

This part describes some of the methods we have attempted to cool the APD, and their effectiveness on reducing the dark count rate.

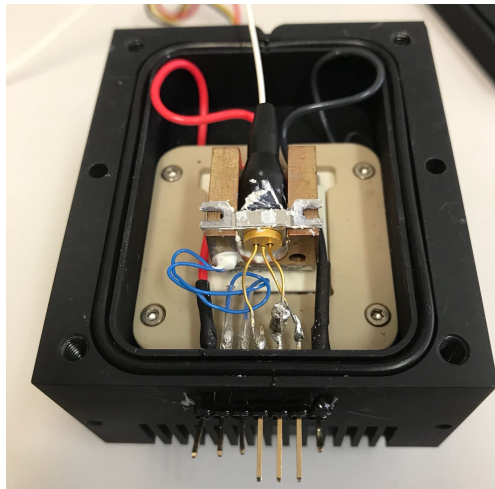


Figure 26: A fully assembled NEC NR8800FS-CB. The copper block is milled to a semi-circle shape at the centre so as to fit the shape of the APD. The APD is passively quenched by a ballast resistor of 390 k Ω .

We started off with a basic configuration by inserting the diode into a copper block which is soldered onto a three-stage Peltier (Ferrotec 9530/119/045 B) and then housed in an anodised aluminium heatsink, as shown in Figure 26. The temperature of the APD is measured by a 10 k Ω thermistor (EPCOS B57861S) in contact with the copper block.

The lowest stable temperature attained with this configuration is -35 $^{\circ}\text{C}$ with a breakdown voltage of 68.7 V. Any Peltier current beyond 4 A will cause the APD to undergo thermal overrun ³, but any Peltier current below 4 A is insufficient to

³The point whereby a small increment in cooling current will in turn lead to an increase in

cool the APD to beyond -35°C . This inefficiency in cooling is suspected to be due to conduction of heat inside the box.

Polyurethane foam

The next attempt is to fill the box with Polyurethane (PU) foam. PU foam is a polymer composed of organic units joined by carbamate (urethane) links; the foam exists as a semi-liquid form when it is output from a compressed can and gets cured when in contact with air to become a solid (similar to styrofoam) where there are small air holes inside. This will reduce the conduction inside the box since air is a bad conductor of heat.

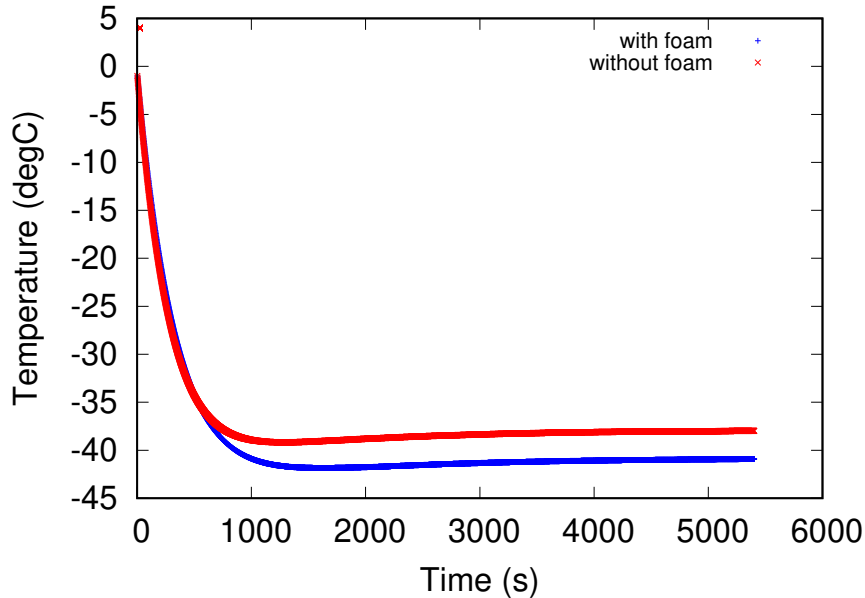


Figure 27: Temperature stability of APD with and without PU foam over time at constant current mode of 4 A.

The anodised aluminium box (without diode) is filled with PU foam and operated at constant current mode with 4 A of current. It was observed that the box with PU foam can reach a stable temperature of approximately -41°C , exhibiting slightly better cooling ability than without any PU foam.

stage temperature. This could be due to limitations in the TEC efficiency or heatsink limitations such as thermal resistance between the peltier stage and the heatsink, and the heatsink inability to dissipate heat efficiently.

Stirling fridge

To achieve even lower temperatures, the APD was put into a Stirling fridge (Stirling Ultracold Shuttle ULT-25NE) which has a temperature set range of $-20\text{ }^{\circ}\text{C}$ to $-86\text{ }^{\circ}\text{C}$. To do so, the APD is housed differently, where the diode is mounted directly onto an aluminium heatsink with respective adapters as shown in Figure 28, and placed inside the freezer chamber of the Stirling fridge. The temperature of the APD is measured by a PT100 sensor (compatible with measurement of temperatures lower than $-50\text{ }^{\circ}\text{C}$.) in contact with the aluminium heatsink.

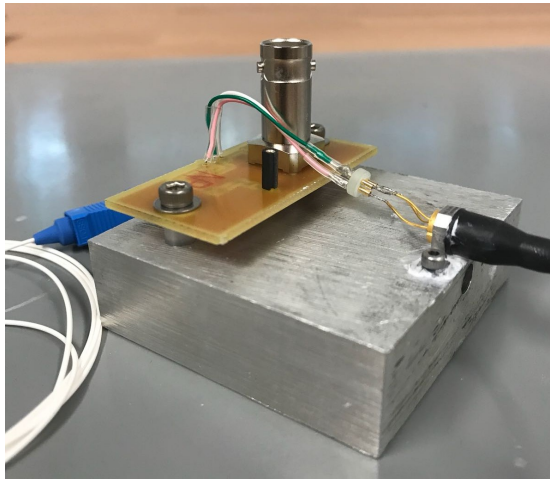


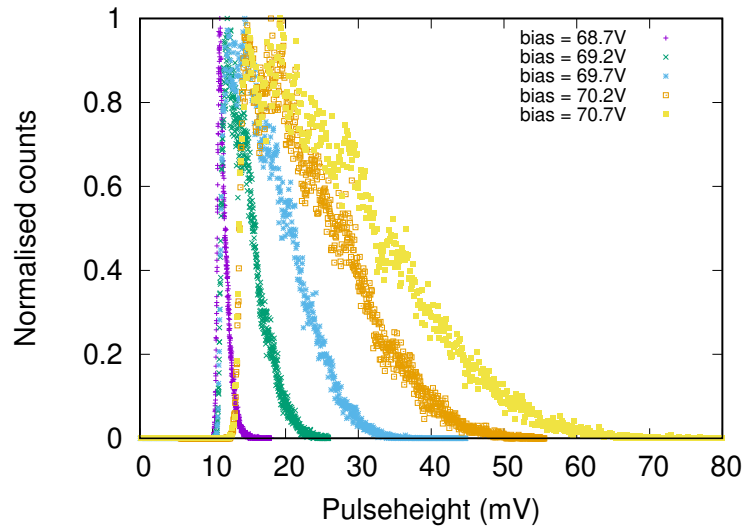
Figure 28: An assembled NEC8800 that will be placed inside the Stirling fridge. The output of the APD is read through a coaxial cable to reduce noise picked up from the fridge.

The lowest temperature attained with this configuration is $-78\text{ }^{\circ}\text{C}$ with a breakdown voltage of 62.3 V .

Pulse height

The histograms of pulse height at varying bias voltages are shown in Figure 29. It is observed to behave fairly similar to that of Renesas NR8360JP-BC. In addition, we see that the pulses are noisier at colder temperatures as represented by a wider width of the histogram. This is suspected to be due to the APD picking up additional noise from the Stirling fridge.

(a) Temperature of -35°C



(b) Temperature of -78°C

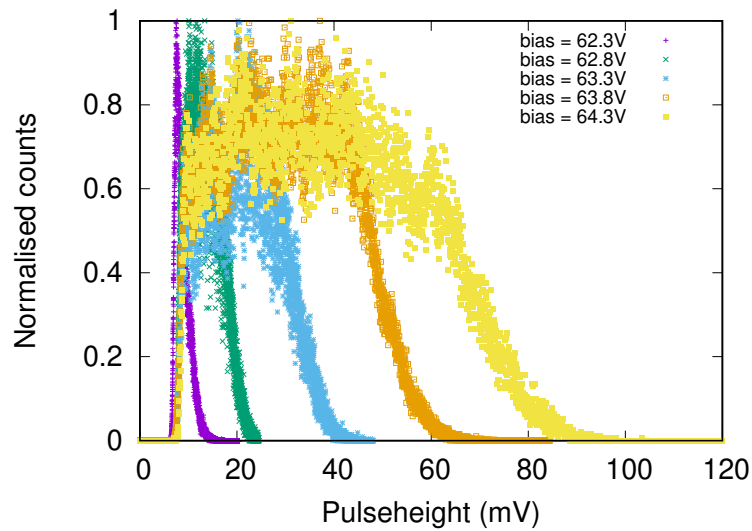


Figure 29: Histogram of pulseheight at varying bias voltages of NR8800FS-CB. A temperature of -35°C is attained with Peltier cooling, while a temperature of -78°C is attained with Stirling fridge. The trigger level on the oscilloscope was set to 6 mV.

Dark count rate

The dark count rate as a function of reverse bias voltage at the two temperatures is shown in Figure 30.

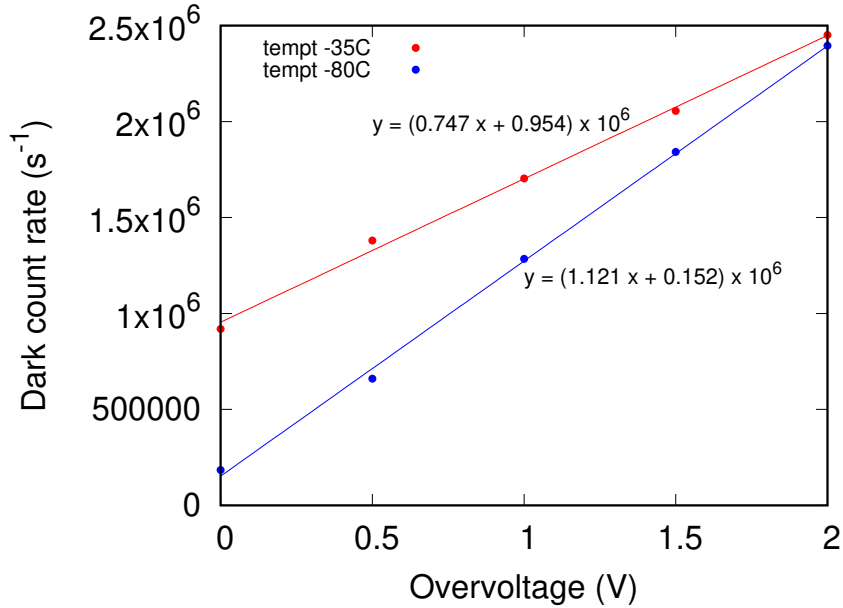


Figure 30: Dark count rate against reverse bias voltages NR8800FS-CB. The reference level on the discriminator card was set to 9mV. The dark count rate is obtained by measuring the dark counts for a total of 1 minute and averaged. A temperature of -35°C is attained with Peltier cooling, while a temperature of -78°C is attained with Stirling fridge.

It seems that despite cooling the APD to -80°C , the dark count rate still remain high at $184,000\text{ s}^{-1}$. This implies that this linear APD is not suitable for light detection at single photon levels despite operating it in Geiger mode. On the other hand, a reduction of dark count rate shows that the high dark count rate observed previously is partly due to thermal excitations. This also shows that the Stirling fridge is one effective way to cool APDs to achieve improvements in dark count rate.

4 Breakdown flash

It was found that during the avalanche process, free electrons can be re-absorbed and emit fluorescence light [29, 44] known as breakdown flash (BDF). It has been observed in Silicon APDs [23], which spans over a spectral distribution of 700 nm to 1000 nm, and has also been investigated in InGaAs APDs at specific spectral windows from 1530 nm to 1600 nm [25, 26, 27]. It is important to investigate the breakdown flash characteristics of APDs as it can cause false readings in an experiment and in the context of QKD, be a potential side-channel attack which can hinder the security of the system.

Breakdown flash is a discharge of light due to the recombination of electrons and holes in the APD junction during the avalanche breakdown process. When an electron transits from the conduction band into a hole in the valence band, a recombination process occurs and an electron-hole pair disappears. In a direct bandgap semiconductor like InGaAs, the energy of recombination can be released as a photon of light.

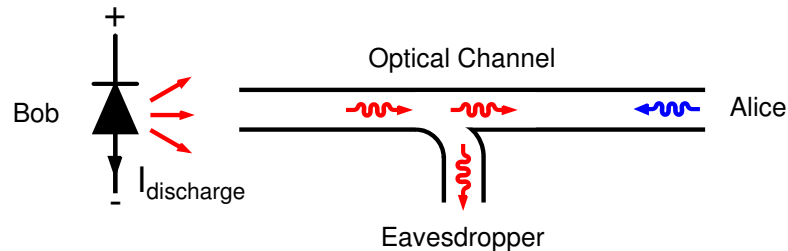


Figure 31: Representation of an eavesdropper attack exploiting the breakdown flash in a QKD setting.

In the context of QKD, the eavesdropper may extract timing and/or polarization information of the detected photons by observing the breakdown flash leaked back to the optical channel [23]. Eve can passively measure any breakdown flash arising from the avalanching carriers to learn the detected bit value as shown in Figure 31. Breakdown flash can also cause false readings in photon correlation experiments such as those used in single atom spectroscopy and single photon interferometry experiments where a breakdown flash off one detector may be observed in the other detector.

4.1 Detection of Breakdown Flash

In this section, we are only looking at the breakdown flash characteristics of the ID Quantique, ID220 modules because, based on the characterisation of the detectors, it appears to be the most promising detector thus far to be applied to the QKD system.

The setup for detecting breakdown flash is shown in Figure 32. The output signals from the two APDs are connected to two channels of an oscilloscope, where the oscilloscope trigger on the signal from APD2 and record the arrival time of the signal from APD1 within the next 250 ns with a time resolution of 100 ps. An electrical delay is applied to APD1 to offset the signal arrival time such that only positive time differences are recorded by the oscilloscope. The experimental setup is kept in dark conditions, such that the breakdown flash is only caused by dark breakdown events in the APDs. A dark breakdown event is a thermally induced avalanche breakdown in the APD, hence it emits the same breakdown flash light as what would be generated in a photodetection event [45].

With each fibre-coupled detectors APD1 and APD2 acting as both a source and detector, the event timings are recorded by the oscilloscope over an integration time of 12 hours and the results are histogrammed as shown in red in Figure 34.

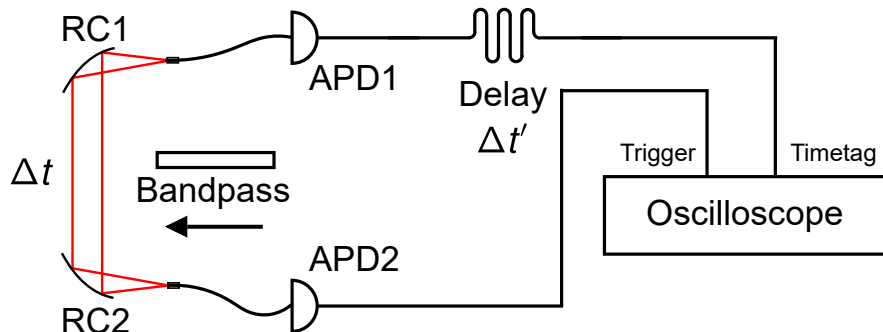


Figure 32: Setup for breakdown flash detection. The output signals are sent to the oscilloscope (Lecroy Waverunner 640 Zi) with an electrical delay of $\Delta t' \approx 127$ ns applied to APD1. The coincidence events of APD1 breakdown flash and APD2 signal, and the other way round is measured.

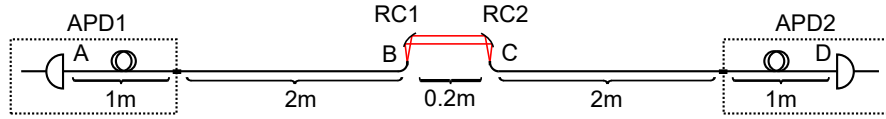


Figure 33: Schematics of the length of fibre patchcords. The APDs are optically coupled through free space by a pair of reflective collimators (RC1 and RC2) placed approximately 0.2m apart, with an overall transmission of 89% (including fibre losses). Each APD is connected to the oscilloscope through 3 meters of optical fibre; 2 meters patchcord + 1 meter fibre in the detector module. The time for a photon to travel the optical path from point A to point D is approximately $\Delta t \approx 32.5$ ns.

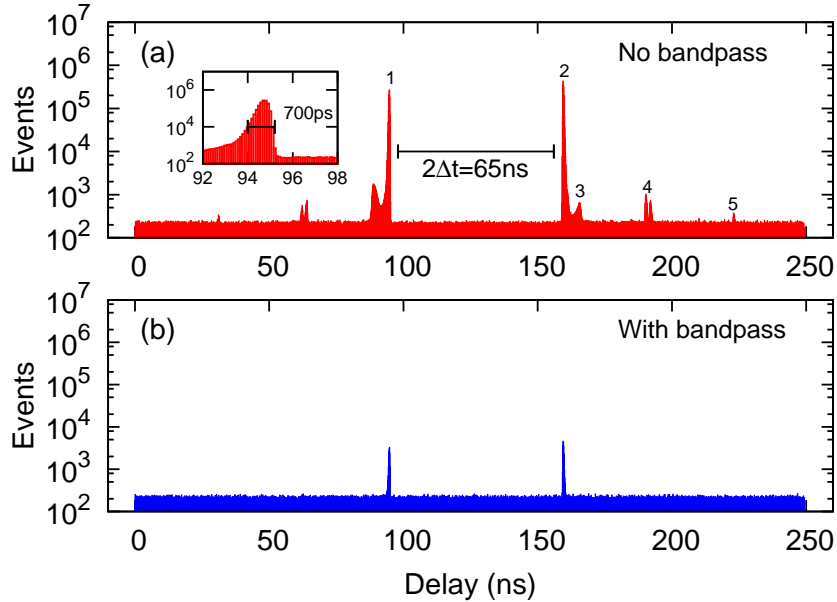


Figure 34: Histogram of signal arrival times from APD1 recorded by an oscilloscope, with and without bandpass filters. The respective peaks indicate the following: (1) Breakdown flash of APD1 (2) Breakdown flash of APD2 (3) Afterpulsing of APD1 (4) Back reflection of breakdown flash of APD2 (5) Tertiary breakdown flash of APD2.

The measurement starts when a dark breakdown event in APD2 triggered the oscilloscope at $t = 0$ s. This breakdown event then creates a breakdown flash in APD2, which travels from APD2 to APD1 then to the oscilloscope, where the arrival time is then recorded. This would imply that the breakdown flash of APD2 travels a route of D-C-B-A-oscilloscope, which translate to a travelling time of $t_2 = \Delta t + \Delta t' \approx 159.5$ ns. On the other hand, a breakdown event in APD1 will send a signal to the oscilloscope which takes up a travelling time of $\Delta t' \approx 127$ ns. In parallel, the breakdown event creates a breakdown flash which travels to APD2 in time $\Delta t \approx 32.5$ ns, and triggers the oscilloscope as $t = 0$. This would imply that the total time taken for the breakdown flash of APD1 to be recorded is $t_{\text{APD1}} = \Delta t' - \Delta t \approx 94.5$ ns.

Looking at Figure 34, the location of the prominent peak 1 and peak 2 would correspond to the breakdown flash events of APD1 and APD2 respectively, where each peak has a full width at half maximum (FWHM) of approximately 700 ps. The timing separation between the two peaks is approximately $2\Delta t \approx 65$ ns, matching twice the optical transit time from A to D.

Peak 3, which is the tail of peak 2, is suspected to be afterpulsing signals of APD2 [26]. Afterpulses occur when carriers are released from traps in the multiplication region and successfully trigger an avalanche [46]. This goes the same for the tail of peak 1.

Looking closely at peak 4, we observe two small peaks which are possibly due to the back reflections of photons at the reflective collimators from a secondary breakdown flash in APD1 (triggered by breakdown flash photons from APD2), which follow a path D-C-B-A-B-A or D-C-B-A-C-A. The timing difference between peak 4 and peak 2 is about 31 ns, which corresponds to a fibre length of about 6 meters (from point A to B/C then back to A as shown in Figure 33).

Peak 5, which is approximately 64 ns away from peak 2, and is suspected to be a tertiary breakdown from APD2 (triggered by photons from the secondary breakdown flash in APD1) since this timing difference matches a fibre length of about 12 m (from point A to D then back to A as shown in Figure 33).

4.2 Elimination of breakdown flash

Knowing the presence of breakdown flash in the detectors, the next step would be to implement ways to reduce or eliminate them, and the easiest way would be to use a bandpass filter to attenuate the flashes. Since the detectors are manufactured for telecom wavelengths, we attempt to use bandpass filter centred at 1300 nm to see its effectiveness. The transmission profile of the bandpass filter is shown in Figure 35.

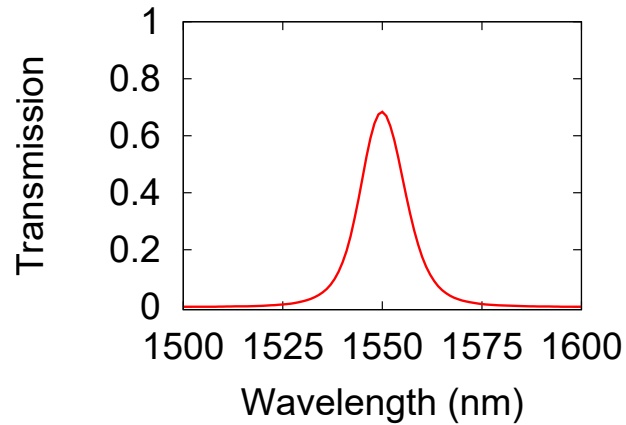


Figure 35: The transmission profile of the bandpass filter.

The same coincidence measurement was repeated with a bandpass filter inserted between RC1 and RC2. The events timing histogram is shown in blue in Figure 34. We observe that the prominent peak 1 and peak 2 are suppressed by a factor of about 100, while the other small peaks are no longer observable.

4.3 Breakdown Flash Probability

In this section, we measure the BDF probability of the APD, which we define as

$$\text{BDF Probability} = \frac{\text{number of BDF events per time}}{\text{count rate of APD}}. \quad (20)$$

To determine the absolute probability of detecting a breakdown flash event, we replace the oscilloscope with a hardware coincidence stage. This is because the recording of timing histograms with the oscilloscope does not directly permit the determination of absolute detection rates for breakdown flash photons, for the histogram processing disables data taking for an unpredictable time. The modified setup is as shown in Figure 37.

Similar to the coincidence measurement done in Section 4.1, a breakdown event in APD1 sends a breakdown signal and a breakdown flash signal to the coincidence stage. Here, the electrical delay ($\Delta t'$) is applied such that it matches the photon traveling time Δt . This would cause the breakdown signal from APD1 and its breakdown flash signal to arrive at the coincidence stage within a coincidence window of 500 ps. Such a coincidence event indicates a breakdown flash emitted by APD1 detected by APD2. The measurement is done through a hardware counter, avoiding the dead time of the oscilloscope in data processing.

The number of breakdown flash events emitted by APD2 is measured in the same manner, except that the same electrical delay is now applied to signals from APD2. For each configuration, we continuously record the number of coincidences for 12 hours. Subsequently, the measurement is repeated with bandpass filters. We find a rate of $44.4 \pm 2.2 \text{ s}^{-1}$ from APD1 to APD2, and $22.2 \pm 1.6 \text{ s}^{-1}$ from APD2 to APD1. Normalising the coincidences by the count rate of the emitting APDs, as shown in equation 20, the breakdown flash probabilities are tabulated in Table 2.

We then estimate the rate of accidental coincidences by blocking the optical path between the APDs, yielding a rate of $0.032 \pm 0.057 \text{ s}^{-1}$, with dark count rates of $(9.55 \pm 0.18) \times 10^3 \text{ s}^{-1}$ and $(5.46 \pm 0.20) \times 10^3 \text{ s}^{-1}$ for APD1 and APD2 respectively.

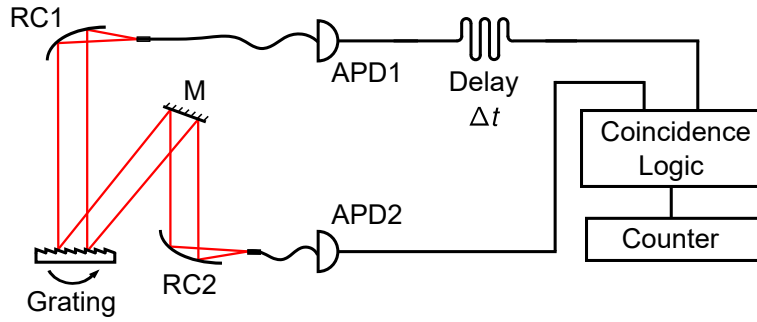


Figure 36: Setup for a coincidence measurement to determine the rate of detecting breakdown flashes from APD1. To measure the breakdown flash rates from APD2, the electrical delay is swapped to connect to APD2.

Emitting APD	Without bandpass	With bandpass
APD 1	$0.44\% \pm 0.02\%$	$0.0057\% \pm 0.0033\%$
APD 2	$0.42\% \pm 0.03\%$	$0.0049\% \pm 0.0023\%$

Table 2: Breakdown flash probability with and without bandpass filters.

The results in Table 2 shows that applying bandpass filters can reduce breakdown flash probability by a factor of close to 100. Coupled with the results in Figure 34, this suggests that spectral filtering could be used as a countermeasure to effectively reduce the breakdown flash in a QKD scenario.

4.4 Spectral Distribution

To achieve better effects of spectral filtering, the spectral distribution of the breakdown flash is investigated. The spectral distribution of the breakdown flash is measured by inserting a monochromator with a grating in between the two reflective collimators. The modified setup is shown in Figure 37.

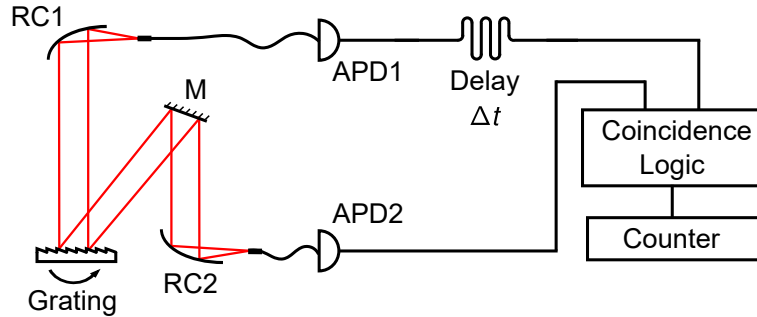


Figure 37: Setup for measuring the spectral distribution of the breakdown flash. A monochromator consisting of a reflective grating (600 lines/mm, blazed at $1.25 \mu\text{m}$) and a pair of reflective collimators (RC1 and RC2) is inserted in the optical path between the two APDs.

The grating is rotated to select the transmission wavelength between them. To estimate the spectral resolution of the monochromator, we measure the instrument response to a 1310 nm single-mode diode laser, and find a full width at half maximum (FWHM) of 3.3 nm. For the first-order diffraction of the same 1310 nm light, we observe a transmission of 51 % from the optical path between APD1 to APD2.

We sampled 84 wavelengths ranging from 1000 nm to 2000 nm with a grating angle incrementation of 0.28° . We perform same coincidence measurement as with the single bandpass in the optical path, but now with an integration time of 30 minutes. The results are shown in Figure 38.

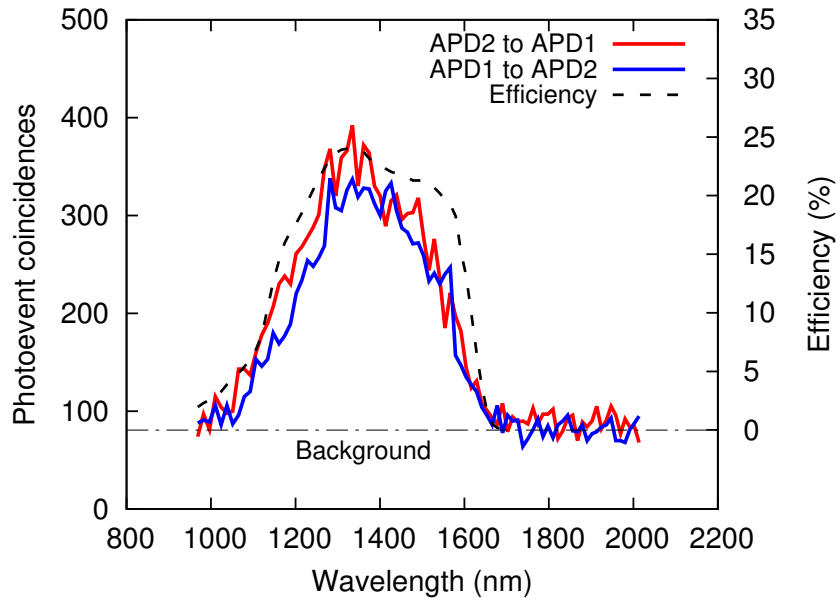


Figure 38: Spectral distribution of the InGaAs APD breakdown flash.

The results are not corrected for the transmission efficiency of the monochromator, nor the wavelength-dependent detection efficiencies of the two APDs. From the results, we see that the coincidence events span a wide range from 1000 nm to 1600 nm, with a maximum at about 1300 nm. We are unable to detect spectral components outside the 1000 nm — 1650 nm band.

It is also observed that the spectra look similar to the spectral dependency of the nominal quantum efficiency of the APD provided by the manufacturer. The close match of spectral sensitivity and observed spectrum of the flash suggests that the spectrum could be relatively flat over the whole region we are able to observe, and could even extend beyond that sensitivity range. A more comprehensive measurement of the actual spectrum would require more wide-band photodetectors such as the recently improved superconducting nanowire detectors [47].

5 Conclusion and outlook

This thesis described a systematic way to characterise InGaAs single photon avalanche photodiode from four different manufacturers: ID Quantique, Laser Components, Princeton Lightwave, Renesas. The characterisation focuses on the following characteristics of an APD: breakdown voltage, pulse height, dark count rate, detection efficiency, and timing jitter.

The characterisation started off with the single photon detection modules from ID Quantique, ID220, where we observe differing performances between two similar detection modules. The characterisation of Count Q from Laser Components, was not fruitful, where we see APD deadtime behaviour conflicting with the respective APD settings. It is thus important for one to characterise every APD especially when detection efficiency and timing jitter is crucial to the experimental results. The performances reflected in the datasheet should only be taken as a reference.

The thesis continues on with the characterisation of Princeton Lightwave PGA-016u-1550TFT which is cheaper but does not exhibit better detection efficiency (4.5%) than ID220 modules. Going down the price list, we also characterised the single photon detection capability of Renesas NR8360JP-BC and NR8800FS-CB, which are APDs manufactured for linear mode operation. In Section 3.2.3, we attempt different methods to cool the Renesas APDs and the lowest temperature attained was $-78\text{ }^{\circ}\text{C}$ with a Stirling fridge. Though cooled to very low temperature, the Renesas APDs display high dark count rate in the order of 10^5 s^{-1} . A high dark count rate can be attributed to the defects in the semiconductor structure that lead to thermally activated charge carriers.

Comparing these detectors, ID220 appears to be the most promising detector to be applied to the QKD system; it has dark count rate in the order of 10^3 s^{-1} , detection efficiency of up to 28%, and a timing jitter of less than 100 ps. Cheaper alternatives like the APD bare diodes do not have performance that match up to that of ID220's, however, their performances could be enhanced with good engineering and packaging. From the characterisation result, it seems that the low detection efficiency is due to a high dark count rate of the APDs, as seen from the reduction in dark count rate when the temperature of the Renesas diodes is

lowered. However, the lowering of temperature is done at the expense of even higher noise. The outlook of this characterisation work would be to reduce the dark count rate of these APDs without raising the noise. One possible idea would be through annealing of the APDs.

In the last part of the thesis, we characterized the breakdown flash from two ID220 using a coincidence measurement, and obtain a lower bound for the probability of detecting a breakdown flash of approximately 0.4%. Given that these APDs have a nominal efficiency of about 10%, the breakdown flash could contain at least 0.04 photons emerging from the fibre connector of the devices. This may result in a considerable amount of information leakage that has to be considered in practical QKD implementations. Moreover, light emission for electron-hole recombinations in direct bandgap semiconductors like InGaAs is more likely to happen than in indirect bandgap semiconductors like Silicon. Thus, measures to suppress the breakdown flash should be implemented.

The most direct method would be through spectral filtering, where we attempt to suppress the breakdown flash by applying a spectral filter in front of an APD, where we see the breakdown flash probability reduced by a factor of 100. We also measured the spectral distribution of the breakdown flash and it appears to be relatively wide. Thus, spectral filtering seems to be a suitable countermeasure to prevent potential information leakage through the breakdown flash in a QKD scenario, similar findings in [25].

In conclusion, we have described a systematic way to characterise InGaAs APDs, and shown a way to investigate breakdown flash. This work will serve as a reference for single photon experiments using the aforementioned detectors.

References

- [1] C. H. Bennett, F. Bessette, G. Brassard, L. Salvail, and J. Smolin, “Experimental quantum cryptography,” *J. Cryptol.*, vol. 5, pp. 3–28, Jan. 1992.
- [2] A. K. Ekert, “Quantum cryptography based on bell’s theorem,” *Phys. Rev. Lett.*, vol. 67, pp. 661–663, Aug 1991.
- [3] N. Gisin, G. Ribordy, W. Tittel, and H. Zbinden, “Quantum cryptography,” *Rev. Mod. Phys.*, vol. 74, pp. 145–195, Mar 2002.
- [4] W. K. Wootters and W. H. Zurek, “A single quantum cannot be cloned,” *Nature*, vol. 299, pp. 802–803, 1982.
- [5] D. Renker, “Photosensors,” *Nuclear Instruments and Methods in Physics Research Section A: Accelerators, Spectrometers, Detectors and Associated Equipment*, vol. 527, no. 1, pp. 15–20, 2004.
- [6] P. Walther, K. J. Resch, T. Rudolph, E. Schenck, H. Weinfurter, V. Vedral, M. Aspelmeyer, and A. Zeilinger, “Experimental one-way quantum computing,” *Nature*, vol. 434, no. 169, 2005.
- [7] L. S. Dolin and A. G. Luchinin, “Water-scattered signal to compensate for the rough sea surface effect on bottom lidar imaging,” *Appl. Opt.*, vol. 47, pp. 6871–6878, Dec 2008.
- [8] B. Cabrera, R. M. Clarke, P. Colling, A. J. Miller, S. Nam, and R. W. Romani, “Detection of single infrared, optical, and ultraviolet photons using superconducting transition edge sensors,” *Applied Physics Letters*, vol. 73, no. 6, pp. 735–737, 1998.
- [9] G. N. Goltsman, O. Okunev, G. Chulkova, A. Lipatov, A. Semenov, K. Smirnov, B. Voronov, A. Dzardanov, C. Williams, and R. Sobolewski, “Picosecond superconducting single-photon optical detector,” *Applied Physics Letters*, vol. 79, no. 6, pp. 705–707, 2001.
- [10] M. Caloz, M. Perrenoud, C. Autebert, B. Korzh, M. Weiss, C. Schnenberger, R. J. Warburton, H. Zbinden, and F. Bussires, “High-detection efficiency and low-timing jitter with amorphous superconducting nanowire single-photon detectors,” *Applied Physics Letters*, vol. 112, no. 6, p. 061103, 2018.

- [11] J. Lee, L. Shen, A. Cer, T. Gerrits, A. E. Lita, S. W. Nam, and C. Kurtsiefer, “Multi-pulse fitting of transition edge sensor signals from a near-infrared continuous-wave source,” *arXiv:1808.08830*, Aug 2018.
- [12] H. G. Irwin K., *Cryogenic Particle Detection*. Berlin, Heidelberg: Springer, 09 July 2005.
- [13] H.-L. Yin, T.-Y. Chen, Z.-W. Yu, H. Liu, L.-X. You, Y.-H. Zhou, S.-J. Chen, Y. Mao, M.-Q. Huang, W.-J. Zhang, H. Chen, M. J. Li, D. Nolan, F. Zhou, X. Jiang, Z. Wang, Q. Zhang, X.-B. Wang, and J.-W. Pan, “Measurement-device-independent quantum key distribution over a 404 km optical fiber,” *Phys. Rev. Lett.*, vol. 117, p. 190501, Nov 2016.
- [14] B. Robert, A. J. Miguel, and L. Alexander, “Progress in satellite quantum key distribution,” *npj Quantum Information*, vol. 3, Aug 2017.
- [15] C. Holloway, E. Meyer-Scott, C. Erven, and T. Jennewein, “Quantum entanglement distribution with 810 nm photons through active telecommunication fibers,” *Opt. Express*, vol. 19, pp. 20597–20603, Oct 2011.
- [16] B. Fröhlich, M. Lucamarini, J. F. Dynes, L. C. Comandar, W. W.-S. Tam, A. Plews, A. W. Sharpe, Z. Yuan, and A. J. Shields, “Long-distance quantum key distribution secure against coherent attacks,” *Optica*, vol. 4, pp. 163–167, Jan 2017.
- [17] B. Korzh, C. C. W. Lim, R. Houlmann, N. Gisin, M. J. Li, D. Nolan, B. Sanguinetti, R. Thew, and H. Zbinden, “Provably secure and practical quantum key distribution over 307km of optical fibre,” *Nature Photonics*, vol. 9, p. 163168, Feb. 2015.
- [18] M. Lucamarini, K. A. Patel, J. F. Dynes, B. Fröhlich, A. W. Sharpe, A. R. Dixon, Z. L. Yuan, R. V. Penty, and A. J. Shields, “Efficient decoy-state quantum key distribution with quantified security,” *Opt. Express*, vol. 21, pp. 24550–24565, Oct 2013.
- [19] A. Boaron, G. Boso, C. V. Davide Rusca, C. Autebert, M. Caloz, M. Perrenoud, G. Gras, F. Bussières, M.-J. Li, D. Nolan, A. Martin, and H. Zbinden, “Secure quantum key distribution over 421 km of optical fiber,” *arXiv:1807.03222v1*, Jul 2018.

- [20] O. S. Abdulwahid¹, J. Sexton, I. Kostakis, K. Ian, and M. Missous, “Physical modelling and experimental characterisation of InGaAs/InP avalanche photodiode for 10Gb/s data rates and higher,” *IET Optoelectronics*, Oct 2017.
- [21] B. Korzh, T. Lunghi, K. Kuzmenko, G. Boso, and H. Zbinden, “Afterpulsing studies of low-noise InGaAs/InP single-photon negative-feedback avalanche diodes,” *Journal of Modern Optics*, vol. 62, no. 14, pp. 1151–1157, 2015.
- [22] L. Z. Jie, “Characterisation of single photon detectors,” *NUS Honours Thesis*, 2016.
- [23] C. Kurtsiefer, P. Zarda, S. Mayer, and H. Weinfurter, “The breakdown flash of silicon avalanche photodiodes-back door for eavesdropper attacks?,” *Journal of Modern Optics*, vol. 48, pp. 2039–2047, Nov 2001.
- [24] P. V. P. Pinheiro, P. Chaiwongkhot, S. Sajeed, R. T. Horn, J.-P. Bourgoin, T. Jennewein, N. Lütkenhaus, and V. Makarov, “Eavesdropping and countermeasures for backflash side channel in quantum cryptography,” *Opt. Express*, vol. 26, pp. 21020–21032, Aug 2018.
- [25] A. Meda, I. P. Degiovanni, A. Tosi, Z. Yuan, G. Brida, and M. Genovese, “Quantifying backflash radiation to prevent zero-error attacks in quantum key distribution,” *Light: Science & Applications*, vol. 6, p. e16261, Dec 2016.
- [26] L. Marini, R. Camphausen, C. Xiong, B. Eggleton, and S. Palomba, “Breakdown flash at telecom wavelengths in direct bandgap single-photon avalanche photodiodes,” *Photonics and Fiber Technology 2016 (ACOFT, BGPP, NP)*, 2016.
- [27] F. Acerbi, A. Tosi, and F. Zappa, “Avalanche current waveform estimated from electroluminescence in InGaAs/InP SPADs,” *IEEE Photonics Technology Letters*, vol. 25, pp. 1778–1780, Sept 2013.
- [28] S. Verghese, K. A. McIntosh, R. J. Molnar, L. J. Mahoney, R. L. Aggarwal, M. W. Geis, K. M. Molvar, E. K. Duerr, and I. Melngailis, “GaN avalanche photodiodes operating in linear-gain mode and Geiger mode,” *IEEE Transactions on Electron Devices*, vol. 48, pp. 502–511, March 2001.

- [29] R. Hadfield, “Single-photon detectors for optical quantum information applications,” *Nature Photonics*, vol. 3, pp. 696–705, 12 2009.
- [30] Z. A. Waris, J. S. Koduru, S. Mario, and U. Rupert, “Comparative study of afterpulsing behavior and models in single photon counting avalanche photo diode detectors,” *Scientific Reports*, vol. 8, no. 1, p. 479, 2018.
- [31] K. E. Jensen, P. I. Hopman, E. K. Duerr, E. A. Dauler, J. P. Donnelly, S. H. Groves, L. J. Mahoney, K. A. McIntosh, K. M. Molvar, A. Napoleone, D. C. Oakley, S. Verghese, C. J. Vineis, and R. D. Younger, “Afterpulsing in geiger-mode avalanche photodiodes for 1.06 μ m wavelength,” *Applied Physics Letters*, vol. 88, no. 13, p. 133503, 2006.
- [32] C.-C. Chen, “Effect of detector dead time on the performance of optical direct-detection communication links,” in *The Telecommunications and Data Acquisition Report* (E. C. Posner, ed.), May 1988.
- [33] M. Stipčević, H. Skenderović, and D. Gracin, “Characterization of a novel avalanche photodiode for single photon detection in vis-nir range,” *Opt. Express*, vol. 18, pp. 17448–17459, Aug 2010.
- [34] J. Y. Cheung, C. J. Chunnillal, P. J. Thomas, J. R. Mountford, and N. P. Fox, “Photon-counting: measurement challenges,” in *International Congress on Optics and Optoelectronics*, pp. 65830G–65830G, International Society for Optics and Photonics, 2007.
- [35] G. M. Williams and A. S. Huntington, “Probabilistic analysis of linear mode vs. Geiger mode APD FPAs for advanced LADAR enabled interceptors,” in *Society of Photo-Optical Instrumentation Engineers (SPIE) Conference Series*, vol. 6220 of , p. 622008, May 2006.
- [36] G. Dietsche, M. Ninck, C. Ortoft, J. Li, F. Jaillon, and T. Gisler, “Fiber-based multispeckle detection for time-resolved diffusing-wave spectroscopy: characterization and application to blood flow detection in deep tissue,” *Appl. Opt.*, vol. 46, pp. 8506–8514, Dec 2007.
- [37] M. Halder, A. Beveratos, R. T. Thew, C. Jorel, H. Zbinden, and N. Gisin, “High coherence photon pair source for quantum communication,” *New Journal of Physics*, vol. 10, no. 2, p. 023027, 2008.

- [38] C. Niclass, A. Rochas, P.-A. Besse, and E. Charbon, “Design and characterization of a cmos 3-d image sensor based on single photon avalanche diodes,” *Solid-State Circuits, IEEE Journal of*, vol. 40, no. 9, pp. 1847–1854, 2005.
- [39] J. G. Rarity, T. E. Wall, K. D. Ridley, P. C. M. Owens, and P. R. Tapster, “Single-photon counting for the 1300–1600-nm range by use of peltier-cooled and passively quenched ingaas avalanche photodiodes,” *Appl. Opt.*, vol. 39, pp. 6746–6753, Dec 2000.
- [40] D. Stucki, G. Ribordy, A. Stefanov, H. Zbinden, J. G. Rarity, and T. Wall, “Photon counting for quantum key distribution with peltier cooled In-GaAs/InP APDs,” *Journal of Modern Optics*, vol. 48, no. 13, pp. 1967–1981, 2001.
- [41] L. You, X. Yang, Y. He, W. Zhang, D. Liu, W. Zhang, L. Zhang, L. Zhang, X. Liu, S. Chen, Z. Wang, and X. Xie, “Jitter analysis of a superconducting nanowire single photon detector,” *AIP Advances*, vol. 3, no. 7, p. 072135, 2013.
- [42] S. Kishimoto, “Pulse-height measurements with a cooled avalanche-photodiode detector,” *Journal of Synchrotron Radiation*, vol. 5, pp. 883–885, May 1998.
- [43] *High-speed photon counting with linear-mode APD receivers*, vol. 7320, 2009.
- [44] R. Newman, “Visible light from a silicon p-n junction,” *Phys. Rev.*, vol. 100, pp. 700–703, Oct 1955.
- [45] W. Shockley and W. T. Read, “Statistics of the recombinations of holes and electrons,” *Phys. Rev.*, vol. 87, pp. 835–842, Sep 1952.
- [46] Y. Kang, D. S. Bethune, W. P. Risk, and Y. H. Lo, “Afterpulsing of single-photon avalanche photodetectors,” in *The 16th Annual Meeting of the IEEE Lasers and Electro-Optics Society, 2003. LEOS 2003.*, vol. 2, pp. 775–776 vol.2, Oct 2003.
- [47] G. N. Gol’tsman, O. Okunev, G. Chulkova, A. Lipatov, A. Semenov, K. Smirnov, B. Voronov, A. Dzardanov, C. Williams, and R. Sobolewski, “Picosecond superconducting single-photon optical detector,” *Applied Physics Letters*, vol. 79, no. 6, pp. 705–707, 2001.